

1 **Heterogeneity and chemical reactivity of the remote troposphere defined by aircraft**
2 **measurements - Corrected**

3 ~~(CORRECTED version of <https://doi.org/10.5194/acp-21-13729-2021>)~~

4 Hao Guo¹, Clare M. Flynn², Michael J. Prather¹, Sarah A. Strode³, Stephen D. Steenrod³,
5 Louisa Emmons⁴, Forrest Lacey^{4,5}, Jean-Francois Lamarque⁴, Arlene M. Fiore⁶, Gus
6 Correa⁶, Lee T. Murray⁷, Glenn M. Wolfe^{3,8}, Jason M. St. Clair^{3,8}, Michelle Kim⁹, John
7 Crounse¹⁰, Glenn Diskin¹⁰, Joshua DiGangi¹⁰, Bruce C. Daube^{11,12}, Roisin Commane^{11,12},
8 Kathryn McKain^{13,14}, Jeff Peischl^{14,15}, Thomas B. Ryerson^{13,15}, Chelsea Thompson¹³,
9 Thomas F. Hanisco³, Donald Blake¹⁶, Nicola J. Blake¹⁶, Eric C. Apel⁴, Rebecca S.
10 Hornbrook⁴, James W. Elkins¹⁴, Eric J. Hintsa^{13,14}, Fred L. Moore^{13,14}, Steven Wofsy¹¹

11 ¹ Department of Earth System Science, University of California, Irvine, CA 92697

12 ² Department of Meteorology, Stockholm University, Stockholm SE-106 91, Sweden

13 ³ Atmospheric Chemistry and Dynamics Laboratory, NASA Goddard Space Flight
14 Center, Greenbelt, MD 20771

15 ⁴ Atmospheric Chemistry Observations and Modeling Laboratory, National Center for
16 Atmospheric Research, Boulder, CO 80301

17 ⁵ Department of Mechanical Engineering, University of Colorado, Boulder, CO 80309

18 ⁶ Department of Earth and Environmental Sciences and Lamont-Doherty Earth
19 Observatory, Columbia University, Palisades, NY 10964

20 ⁷ Department of Earth and Environmental Sciences, University of Rochester, Rochester,
21 NY 14611

22 ⁸ Joint Center for Earth Systems Technology, University of Maryland, Baltimore County,
23 Baltimore, MD 21228

24 ⁹ Department of Geological and Planetary Sciences, California Institute of Technology,
25 Pasadena, CA 91125

26 ¹⁰ Atmospheric Composition, NASA Langley Research Center, Hampton VA 23666

27 ¹¹ John A. Paulson School of Engineering and Applied Sciences, Harvard University,
28 Cambridge, MA 02138

29 ¹² Department of Earth and Planetary Sciences, Harvard University, Cambridge, MA
30 02138

31 ¹³ Cooperative Institute for Research in Environmental Sciences, University of Colorado,
32 Boulder, CO 80309

33 ¹⁴ Global Monitoring Division, Earth System Research Laboratory, NOAA, Boulder, CO
34 80305

35 ¹⁵ Chemical Sciences Division, National Oceanic and Atmospheric Administration Earth
36 System Research Laboratory, Boulder, CO 80305

37 ¹⁶ Department of Chemistry, University of California, Irvine, CA 92697

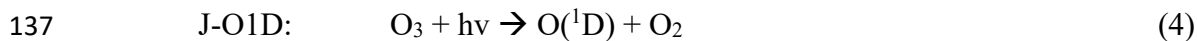
38
39 *Correspondence to:* Hao Guo (haog2@uci.edu) and Michael J. Prather
40 (mprather@uci.edu).

41
42 **Keywords:** Tropospheric Chemistry, Ozone, Methane, Aircraft Observations, NASA
43 ATom

44 **Abstract.** The NASA Atmospheric Tomography (ATom) mission built a photochemical
45 climatology of air parcels based on in situ measurements with the NASA DC-8 aircraft
46 along objectively planned profiling transects through the middle of the Pacific and
47 Atlantic oceans. In this paper we present and analyze a data set of 10 s (2 km) merged
48 and gap-filled observations of the key reactive species driving the chemical budgets of O₃
49 and CH₄ (O₃, CH₄, CO, H₂O, HCHO, H₂O₂, CH₃OOH, C₂H₆, higher alkanes, alkenes,
50 aromatics, NO_x, HNO₃, HNO₄, peroxyacetyl nitrate, other organic nitrates), consisting of
51 146,494 distinct air parcels from ATom deployments 1 through 4. Six models calculated
52 the O₃ and CH₄ photochemical tendencies from this modeling data stream for ATom 1.
53 We find that 80 %–90 % of the total reactivity lies in the top 50 % of the parcels; and 25
54 %–35 %, in the top 10 %, supporting previous model-only studies that tropospheric
55 chemistry is driven by a fraction of all the air. ~~In other words, accurate simulation of the~~
56 ~~least reactive 50 % of the troposphere is unimportant for global budgets.~~ Surprisingly,
57 the probability densities of species and reactivities averaged on a model scale (100 km)
58 differ only slightly from the 2 km ATom 10 s data, indicating that much of the
59 heterogeneity in tropospheric chemistry can be captured with current global chemistry
60 models. Comparing the ATom reactivities over the tropical oceans with climatological
61 statistics from six global chemistry models, we find generally good agreement with the
62 reactivity rates for O₃ and CH₄. ~~In the Pacific but not Atlantic, however, m~~Models
63 distinctly underestimate O₃ production below 2 km relative to the mid-troposphere, and
64 this can be traced to lower NO_x levels than observed. Attaching photochemical
65 reactivities to measurements of chemical species allows for a richer, yet more
66 constrained-to-what-matters, set of metrics for model evaluation.

67
68
69 **Preface.** This paper presents a corrected (CORRECTED-version of the paper published
70 under the same authors and title (sans 'Corrected') as [https://doi.org/10.5194/acp-21-](https://doi.org/10.5194/acp-21-13729-2021)
71 13729-2021. ~~While continuing our analysis of the ATom data we found several major~~
72 ~~mistakes or decision errors. The main conclusions were unchanged except those~~
73 ~~regarding production of O₃, but most of the numbers and many of the figures changed~~
74 ~~slightly. A corrigendum to the original 2021 paper was prepared, but the changes were~~
75 ~~extensive enough so that the ACP editors and the authors decided that a completely new~~
76 ~~paper should be produced and the 2021 paper withdrawn. The errors that were corrected~~
77 ~~are described in this preface and discussed at most briefly in the paper. First, we found~~
78 ~~that measurement errors in PAN and HNO₄ were large (~100 ppt), and when this~~
79 ~~occurred in the lower troposphere, the rapid thermal decomposition released large~~
80 ~~amounts of NO_x. There is no easy fix for this, and we developed a new protocol (RDS*)~~
81 ~~for computing reactivities by allowing the species to thermally decompose before use in~~
82 ~~the model, as described below. This fix greatly reduced O₃ production (P-O3) in the~~
83 ~~lower troposphere. A second NO_x problem involved the propagation of polluted profiles~~
84 ~~from the Los Angeles basin to gap filling over the tropical eastern Pacific. This~~
85 ~~correction resulted in the update of the Modeling Data Stream to version 2b. These NO_x~~
86 ~~errors cause noticeable changes in reactivities, especially P-O3. Other decision errors led~~
87 ~~us to decrease the southern latitude extent of the Atlantic and Pacific transects from 54° S~~
88 ~~to 53° S to avoid spurious parcels being included. Also, cosine of latitude weighting was~~
89 ~~applied to data for all figures and tables. The UCI model now includes all higher alkanes~~

136



138



140

141

142 Models also reported the change in O_3 over 24 h, and these match the P- O_3 minus L- O_3
143 values over the Pacific basin (a focus of this study). The models showed a wide range in
144 the three Rs average profiles across latitudes over the Pacific basin, as well as 2D
145 probability densities (PDs) for key species such as NO_x ($NO + NO_2$) versus HOOH. A
146 large part of the model differences was attributed to the large differences found in
147 chemical composition rather than the calculation of rates from that composition. We
148 found that single transects from a model through the tropical Pacific at different
149 longitudes produced nearly identical 2D PDs, but these PDs were distinctly different
150 across models. This result supported the premise that the ATom PDs would provide a
151 useful metric for global chemistry models.

152

153 In P2017, we established a method for running the chemistry modules in the CTMs and
154 CCMs with an imposed chemical composition from aircraft data: the ATom run, or “A
155 run”. In the A run, the chemistry of each grid cell does not interact with its neighbors or
156 with externally imposed emission sources. Effectively the CTM/CCM is initialized and
157 run for 24 h without transport, scavenging or emissions. Aerosol chemistry is also turned
158 off in the A runs. This method allows each parcel to evolve in response to the daily cycle
159 of photolysis in each model and be assigned a 24 h integrated reactivity. The
160 instantaneous reaction rates at the time an air parcel is measured (e.g., near sunset at the
161 end of a flight) do not reflect that parcel's overall contribution to the CH_4 or O_3 budget; a
162 full diel cycle is needed. The A run assumption that parcels do not mix with neighboring
163 air masses is an approximation, and thus for each model we compared the A runs using
164 the model's restart data with a parallel standard 24 h simulation (including transport,
165 scavenging, and emissions). Because the standard grid-cell air moves and mixes, we
166 compared averages over a large region (e.g., tropical Pacific). We find some average
167 biases of order $\pm 10\%$ but general agreement. The largest systematic biases in the A runs
168 are caused by buildup of HOOH (no scavenging) and decay of NO_x (no sources). The A
169 runs are relatively easy to code for most CTM/CCMs and allow each model's chemistry
170 module, including photolysis package, to run normally. The A runs do not distinguish
171 between CTMs and CCMs, except that each model will generate/prescribe its own cloud
172 fields and photolysis rates. Our goal is to create a robust understanding of the chemical
173 statistics including the reactivities with which to test and evaluate the free-running
174 CCMs, and thus we do not try to model the specific period of the ATom deployments.
175 Others may use the ATom data with hindcast CTMs to test forecast models, but here we
176 want to build a chemical climatology.

177

178 The first hard test of the A runs came with the second ATom modeling paper ("How well
179 can global chemistry models calculate the reactivity of short-lived greenhouse gases in
180 the remote troposphere, knowing the chemical composition", Prather et al., 2018, hence
181 P2018). The UCI CTM simulated an aircraft-like data set of 14,880 air parcels along the

182 International Date Line from a separate high-resolution (0.5°) model. Each parcel is
183 defined by the following core species: H_2O , O_3 , NO_x , HNO_3 , HNO_4 , PAN (peroxyacetyl
184 nitrate), CH_3NO_3 , HOOH , CH_3OOH , HCHO , CH_3CHO (acetaldehyde), $\text{C}_3\text{H}_6\text{O}$ (acetone),
185 CO , CH_4 , C_2H_6 , alkanes (C_3H_8 and higher), C_2H_4 , aromatics (benzene, toluene, xylene)
186 and C_5H_8 (isoprene), plus temperature. Short-lived radicals (e.g., OH , HO_2 , CH_3OO)
187 were initialized at small concentrations and quickly reached daytime values determined
188 by the core species. The six CTM/CCMs overwrote the chemical composition of a restart
189 file, placing each pseudo-observation in a unique grid cell according to its latitude,
190 longitude, and pressure. If another parcel is already in that cell, then it is shifted east–
191 west or north–south to a neighboring model cell. For coarse-resolution models, multiple
192 restart files and A runs were used to avoid large location shifts. CTM/CCMs usually
193 have a locked in 24 h integration step starting at 0000 UTC that is extremely difficult to
194 modify in order to try to match the local solar time of observation, especially as it
195 changes along aircraft flights. We tested the results with a recoded UCI CTM to start at
196 1200 UTC but retain the same clouds fields over the day and found only percentage-level
197 differences between a midnight or noon start.

198

199 These A runs averaged over cloud conditions by simulating 5 d in August at least 5 d
200 apart. Assessment of the modeled photolysis rates and comparison with the ATom-
201 measured J values is presented in Hall et al. (2018, hence H2018). All models agreed
202 that a small fraction of chemically hot air parcels in the synthetic data set controlled most
203 of the total reactivity. Some models had difficulty in implementing the A runs because
204 they overwrote the specified water vapor with the modeled value, but this problem is
205 fixed here. In both P2017 and P2018, the GISS-E2 model stood out with the most
206 unusual chemistry patterns and sometimes illogical correlations. Efforts by a co-author
207 to clarify the GISS results or identify errors in the implementation have not been
208 successful. GISS results are included here for completeness in the set of three papers but
209 are not reconciled. Overall, three models showed remarkable inter-model agreement in
210 the three Rs with less than half of the RMSD (root-mean-square difference) as compared
211 with the other models. UCI also tested the effect of different model years (1997 and
212 2015 versus reference year 2016), which varies the cloud cover and photolysis rates, and
213 found an inter-year RMSD about half of that of the core model's RMSD. Thus, there is a
214 fundamental uncertainty in this approach due to the inability to specify the
215 cloud/photolysis history seen by a parcel over 24 h, but it is less than the inter-model
216 differences among the most similar models.

217

218 **2 Introduction**

219

220 The NASA Atmospheric Tomography (ATom) mission completed a four-season
221 deployment, each deployment flying from the Arctic to Antarctic and back, traveling
222 south through the middle of the Pacific Ocean, across the Southern Ocean and then north
223 through the Atlantic Ocean, with near-constant profiling of the marine troposphere from
224 0.2 to 12 km altitude (see Fig. S1). The DC8 was equipped with in situ instruments that
225 documented the chemical composition and conditions at time intervals ranging from <1
226 to about 100 seconds (Wofsy et al., 2018). ATom measured hundreds of gases and
227 aerosols, providing information on the chemical patterns and reactivity in the vast remote

228 ocean basins, where most of the destruction of tropospheric ozone (O₃) and methane
229 (CH₄) occurs. Reactivity is defined here as in P2017 to include the production and loss
230 of O₃ (P-O₃ and L-O₃, ppb/d) and loss of CH₄ (L-CH₄, ppb/d). Here we report on this
231 model-derived product that was proposed for ATom, the daily averaged reaction rates
232 determining the production and loss of O₃ and the loss of CH₄ for 10 s averaged air
233 parcels. We calculate these rates with 3D chemical models that include variations in
234 clouds and photolysis, and then assemble the statistical patterns describing the
235 heterogeneity (i.e., high spatial variability) of these rates and the underlying patterns of
236 reactive gases.

237 Tropospheric O₃ and CH₄ contribute to climate warming and global air pollution (Stocker
238 et al., 2013). Their abundances in the troposphere are controlled largely by tropospheric
239 chemical reactions. Thus, chemistry–climate assessments seeking to understand past
240 global change and make future projections for these greenhouse gases have focused on
241 the average tropospheric rates of production and loss and how these reactivities are
242 distributed in large semi-hemispheric zones throughout the troposphere (Griffiths et al.,
243 2021; Myhre et al., 2014; Naik et al., 2013; Prather et al., 2001; Stevenson, et al., 2006;
244 Stevenson, et al., 2013; Stevenson, et al., 2020; Voulgarakis et al., 2013; Young et al.,
245 2013). The models used in these assessments disagree on these overall CH₄ and O₃
246 reactivities (a.k.a. the budgets), and resolving the cause of such differences is stymied
247 because of the large number of processes involved and the resulting highly heterogeneous
248 distribution of chemical species that drive the reactions. Simply put, the models use
249 emissions, photochemistry, and meteorological data to generate the distribution of key
250 species such as nitrogen oxides (NO_x = NO + NO₂) and hydrogen peroxide (HOOH)
251 (step 1) and then calculate the CH₄ and O₃ reactivities from these species (step 2). There
252 is no single average measurement that can test the verisimilitude of the models.
253 Stratospheric studies such as Douglass et al. (1999) have provided a quantitative basis for
254 testing chemistry and transport, and defining model errors; but few of these studies have
255 tackled the problem of modeling the heterogeneity of tropospheric chemistry. The major
256 model differences lie in the first step, because when we specify the mix of key chemical
257 species, most models agree on the CH₄ and O₃ chemical budgets (P2018). The intent of
258 ATom was to collect an atmospheric sampling of all the key species and the statistics
259 defining their spatial variability, and thus that of the reactivities of CH₄ and O₃.

260 Many studies have explored the ability of chemistry–transport models (CTMs) to resolve
261 finer scales such as pollution layers (Eastham and Jacob, 2017; Rastigejev et al., 2010;
262 Tie et al., 2010; Young et al., 2018; Zhuang et al., 2018), but these have not had the
263 chemical observations (statistics) to evaluate model performance. In a great use of
264 chemical statistics, Yu et al. (2016) used 60 s data (~12 km) from the SEAC⁴RS aircraft
265 mission to compare cumulative probability densities (PDs) of NO_x, O₃, HCHO and
266 isoprene over the Southeast US with the GEOS-Chem CTM run at different resolutions.
267 They identified clear biases at the high and low ends of the distribution, providing a new
268 test of models based on the statistics rather than mean values. Heald et al. (2011)
269 gathered high-resolution profiling of organic and sulfate aerosols from 17 aircraft
270 missions and calculated statistics (mean, median, quartiles) but only compared with the
271 modeled means. The HIAPER Pole-to-Pole Observations (HIPPO) aircraft mission
272 (Wofsy, 2011) was a precursor to ATom with regular profiling of the mid-Pacific

273 including high-frequency 10 s sampling that identified the small scales of variability
274 throughout the troposphere. HIPPO measurements were limited in species, lacking O₃,
275 NO_x and many of the core species needed for reactivity calculations. ATom, with a full
276 suite of reactive species and profiling through the Atlantic basin, provides a wealth of
277 chemical statistics that challenge the global chemistry models.

278 ~~One main task~~ here is the assembly of the modeling data stream (MDS), which
279 provides flight-wise continuous 10 s data (air parcels) for the key reactive species. The
280 MDS is based on direct observations and interpolation methods to fill gaps as
281 documented in the Supplement. Using the [version 0 of the MDS](#), we have six chemical
282 models calculating the 24 h reactivities, producing a reactivity data stream (RDS [version](#)
283 [0](#)) using protocols noted in the Prologue (P2017) and described further in Sect. [3.22](#).
284 There, we describe the updated modeling protocol RDS* necessary to address
285 measurement noise in [PAN and HNO₄, which key species that](#) can be very short-lived. In
286 Sect. 4, we examine the statistics of reactivity over the Atlantic and Pacific oceans,
287 focusing on air parcels with high reactivity; for example, 10% of the parcels produce 25-
288 35% of total reactivity over the oceans. We compare these ATom-1 statistics, species
289 and reactivities with August climatologies from six global chemistry models. In one
290 surprising result, ATom-1 shows a more reactive tropical troposphere than found in most
291 models' climatologies associated with higher NO_x levels than in the models. Section 5
292 concludes that the ATom PDs based on 10s air parcels do provide a valid chemistry
293 metric for global models with 1° resolution. It also presents some examples where ATom
294 measurements and modeling can test the chemical relationships and may address the
295 cause of differences in the O₃ and CH₄ budgets currently seen across the models. With
296 this paper we release the full ATom MDS-2**b** from all four deployments along with the
297 updated RDS-2***b** reactivities from the UCI model.

298 **3 Models and data**

299 **3.1 The modeling data stream (MDS)**

300 The ATom mission was designed to collect a multi-species, detailed chemical
301 climatology that documents the spatial patterns of chemical heterogeneity throughout the
302 remote troposphere. Figure S1 in the Supplement maps the 48 research flights, and the
303 Supplement has tables summarizing each flight. We required a complete set of key
304 species in each air parcel to initialize the models that calculate the CH₄ and O₃
305 reactivities. We choose the key reactive species (H₂O, O₃, CO, CH₄, NO_x, NO_xPSS,
306 HNO₃, HNO₄, PAN, CH₂O, H₂O₂, CH₃OOH, acetone, acetaldehyde, C₂H₆, C₃H₈, *i*-
307 C₄H₁₀, *n*-C₄H₁₀, alkanes, C₂H₄, alkenes, C₂H₂, C₃H₈, benzene, toluene, xylene,
308 CH₃ONO₂, C₂H₅ONO₂, RONO₂, CH₃OH) directly from the ATom measurements and
309 then add corollary species or other observational data indicative of industrial or biomass
310 burning pollution or atmospheric processing (HCN, CH₃CN, SF₆, relative humidity,
311 aerosol surface area (four modes), and cloud indicator). We choose 10 s averages for our
312 air parcels as a compromise and because the 10 s merged data are a standard product
313 (Wofsy et al., 2018). A few instruments measure at 1 s intervals, but the variability at
314 this scale is not that different from 10 s averages (Fig. S2). Most of the key species are
315 reported as 10 s values, with some being averaged or sampled at 30 s or longer such as
316 ~90 s for some flask measurements.

317 Throughout ATom, gaps occur in individual species on a range of timescales due to
318 calibration cycles, sampling rates or instrument malfunction. The generation of the MDS
319 uses a range of methods to fill these gaps and assigns a flag index to each species and
320 data point to allow users to identify direct primary measurements and methods used for
321 gap-filling. Where two instruments measure the same species, the MDS selects a primary
322 measurement and identifies which instrument was used with a flag. The methodology
323 and species-specific information on how the current MDS version 2 (MDS-2) is
324 constructed, plus statistics on the 48 research flights and the 146,494 10 s air parcels in
325 MDS-2 are given in the Supplement.

326 Over the course of this study, several MDS versions were developed and tested, including
327 model-derived RDSs from these versions, some of which are used in this paper. In early
328 ATom science team meetings, there was concern about the accuracy of NO₂ direct
329 measurements when at very low concentrations. A group prepared an estimate for NO_x
330 using the NO and O₃ measurements to calculate a photostationary value for NO₂ and thus
331 NO_x. This PSS-NO_x became the primary NO_x source in version 0 (i.e., MDS-0). ~~The~~
332 ~~numbering of versions initially followed the notation of revisions in the mission data~~
333 ~~archive (MDS_R0, MDS_R1, ...), but this was restrictive and we adopted the simpler~~
334 ~~notation here, but still beginning with version 0.~~ With MDS-0, we chose to gap-fill using
335 correlations with CO to estimate the variability of the missing measurement over the gap.
336 The science team then rejected PSS-NO_x as a proxy, and we reverted to the observed NO
337 + NO₂ ~~for MDS-1, resulting in increased NO_x and reactivities (RDS-1).~~ MDS-1 NO_x
338 values that are 25 % larger on average than in MDS-0 ~~values~~ (unweighted mean of 66 vs.
339 52 ppt). ~~This change, and this affected~~ P-O₃ most and L-CH₄ least. We then estimated
340 errors in the gap-filling and found that CO had little skill as a proxy for most other
341 species. With MDS-2, we optimized and tested the treatments of gap-filling and lower
342 limit of detection, along with other quality controls.

343 ~~MDS-2 is fully documented in the Supplementary Information. After publication and~~
344 ~~W~~with continued analysis of the unusually reactive East Pacific region, we determined
345 that the method of long-gap filling for NO_x resulted in propagation of high NO_x levels
346 from the over-land profiles into the over-water profiles in the tropics. We separated these
347 two set of profiles used for long-gap NO_x filling and created an updated version MDS-
348 2b. This experience points to the importance of having reliable, continuous NO_x
349 measurements.

352 3.2 The reactivity data stream (RDS)

353 The concept of using an MDS to initialize 3D global chemistry models and calculate an
354 RDS was developed in the pre-ATom methodology papers (P2017; P2018). In this
355 paper, we use the original six models for their August chemical statistics, and we use 5 of
356 them plus a box model to calculate the reactivities, see Table 1. The RDS is really a
357 protocol applied to the MDS. It is introduced in the Prologue and the details can be
358 found in P2018. A model grid cell chosen to be close to the measured parcel is initialized
359 with all the core reactive species needed for a regular chemistry simulation. The model is
360 then integrated over 24 h without transport or mixing, without scavenging, and without

361 emissions. Each global model uses its own varying cloud fields for the period to
362 calculate photolysis rates; but the F0AM box model simply takes the instant J-values as
363 measured on the flight and applies a diurnal scaling. We ~~can~~ initialize with the core
364 species and let the radicals (OH, HO₂, RO₂) come quickly into photochemical balance.
365 The 24 h integration is not overly sensitive to the start time of the integration, and thus
366 models do not have to synchronize with the local time of observation (see P2018's Fig.
367 S8 and Table S8).

368 The initial ATom-1 reactivities RDS came from MDS-0 and six of the models in Table 1.
369 Although these RDS-0 model results are now out of date because of the move to MDS-
370 2b, they provide critical ~~This paper was nearly complete when we identified the problem~~
371 ~~with PSS-NO_x. We had gathered enough~~ information on how models agree, or disagree,
372 in calculating the with-RDS using the ATom protocol. Thus we include them here as a
373 cross-model comparison. Given the excellent agreement at the parcel level using three
374 models (GC, GMI, UCI), and with a desire to avoid wasting the community's time, we
375 continued the analysis of MDS-2b with just our local UCI CTM. This decision may need
376 to be revisited. -0;

377 ~~and thus chose to assess MDS-1 with two of the models that closely agreed (GMI and~~
378 ~~UCI). The two models were very close in RDS-0 and also in RDS-1. We then found the~~
379 ~~problems with the CO proxy, and chose to use only the UCI model as a transfer standard~~
380 ~~for the change from MDS-1 to MDS-2 (i.e., RDS-1 to RDS-2). This path avoided much~~
381 ~~extra work by the modeling groups and generated the same information on cross-model~~
382 ~~differences and a robust estimate of changes from RDS-0 to RDS-2.~~

383 Statistics for the three reactivities for six models using MDS-0, ~~2 alternative UCI model~~
384 ~~years using MDS-0, the GMI model using MDS-1 and the UCI model using MDS-2~~ are
385 given in Table 2 and Table S8 for three domains: global (all points), Pacific (oceanic data
386 from 53° S to 60° N) and Atlantic (same constraints as Pacific). ~~UCI MDS-1 is similar to~~
387 ~~UCI MDS-2 and is not shown.~~ The statistics try to achieve equal latitude-by-pressure
388 sampling by weighting each ATom parcel inversely according to the number of parcels in
389 each 10° latitude by 100 hPa bin, and each point is also cosine(latitude) weighted. We
390 calculate the means and medians plus the percent of total reactivity in the top 10 % of the
391 weighted parcels (Table 2) and also the mean reactivity of the top 10 %, percent of total
392 reactivity in the top 50 %, 10 % and 3 % plus the mean *J* values (Table S8).

393 These six-model version 0 statistics are shown alongside the version 2b results using the
394 current UCIZ model but with a new protocol designated RDS*. ~~Unfortunately, while~~
395 ~~investigating sensitivities and uncertainties in the RDS for a future study, we found an~~
396 ~~inconsistency between the reported concentrations of both pernitric acid (HNO₄) and~~
397 ~~peroxyacetyl nitrate (PAN) with respect to the chemical kinetics used in the models.~~
398 ~~High concentrations (100 ppt, attributed to instrument noise) were reported under~~
399 ~~conditions where the thermal decomposition frequency was > 0.4 per hour in the lower~~
400 ~~troposphere (> 253 K for HNO₄ and > 291 K for PAN). Thus, these species instantly~~
401 ~~become NO_x. While these measurements are clearly spurious, there is no easy fix. We~~
402 ~~for this, and we left the species data in the MDS as they were reported, but~~ developed a
403 new protocol, RDS*, that allows to deal with them. ~~Both species are allowed to decay~~
404 ~~for 24 h using their local thermal decomposition rate before being used in the put into the~~

405 model. This protocol avoids most-much of the fast thermal release of NO_x in the lower
406 atmosphere during the first 24 h of the RDS calculation, but does not affect the release of
407 NO_x from photolysis or OH reactions in the upper troposphere where thermal
408 decomposition is inconsequential. It is possible that some of the high concentrations of
409 HNO₄ and PAN in the lower troposphere are real and that we are missing this large
410 source of NO_x with the RDS* protocol, but we find there are no obvious sources of these
411 species in the remote oceanic regions that would produce enough to match the thermal
412 loss. Both this problem and its solution do not affect the initial NO_x values.

413
414 We present the RDS-2b reactivities calculated under the RDS* protocol with the UCI
415 CTM. Unfortunately, these new calculations with the revised protocol (UCI2*, shown in
416 the original published version) are not reproducible and inconsistent with the original
417 CTM version used in P2017, P2018, and the MDS-0 calculations. It appears that either
418 the initial conditions, the ATom-specific version of the UCI CTM, or the retrieval of the
419 24-h average rates is not correct. These problems appeared when we calculated
420 sensitivity coefficients ($\partial \ln R / \partial \ln X$) to understand what species (X) were driving the
421 reactivities. We reverted to the ATom-specific UCI CTM developed by Xin Zhu for
422 P2017 and P2018 with additional diagnostics (designated UCIZ*) as our best results in
423 the final column of Tables 2 and S8. We added diagnostics that give us confidence. We
424 now have confidence in our O₃ reactivities: because the approximate P-O₃ and L-O₃
425 based on the limited reactions (rates 2abd and 3abc above) actually predicts the
426 calculated 24 h O₃ tendency, see Fig. S6. Considering the ocean basin observations only,
427 P-L ranges from -12 to +15 ppb/d. The mean error in P-L is about -0.01 ppb/d, and the
428 root-mean-squared error is about 0.04 ppb/d, convincing us that we have correctly
429 diagnosed the P-O₃ and L-O₃ terms. Following the practice of the GMI model, we also
430 record the initial and 24-hour abundances of all the ATom species to check that nothing
431 unusual altered the species abundance in each cell over the 24 hours. Calculations with
432 the updated RDS* protocol are shown under UCIZ* in the final column of Tables 2 and
433 S8. The mean reactivities noticeably drop relative to UCI2 (50 % for P-O₃, 10 % for L-
434 O₃, and 20 % for L-CH₄), but the percentiles do not change much. We recommend use
435 the use the UCIZ* results as our best, revised estimate of the ATom reactivities.

436 437 **3.3 Inter-model differences**

438
439 Variations in reactivities due to clouds are an irreducible source of uncertainty:
440 predicting the cloud-driven photolysis rates that a shearing air parcel will experience over
441 24 h is not possible here. The protocol uses 5 separated 24 h days to average over
442 synoptically varying cloud conditions. The standard deviation (σ) of the 5 d, as a
443 percentage of the 5 d mean, is averaged over all parcels and shown in Table S9 for the
444 five global models. Three central models (GC, GMI, UCI) show 9 %–10 % $\sigma(J_s)$ values
445 and similar $\sigma(R_s)$ values as expected if the variation in J values is driving the reactivities.
446 Two models (GISS, NCAR) have 12 %–17 % $\sigma(J_s)$, which might be explained by more
447 opaque clouds, but the amplified $\sigma(R)$ values (14 %–32 %) are inexplicable. This
448 discrepancy needs to be resolved before using these two models for ATom RDS analysis.

449

450 Inter-model differences are shown in the parcel-by-parcel root-mean-square (rms)
451 differences for RDS-0 in Table 3. Even when models adopt standard kinetic rates and
452 cross sections (i.e., Burkholder et al., 2015), the number of species and chemical
453 mechanisms included, as well as the treatment of families of similar species or
454 intermediate short-lived reaction products, varies across models. For example, UCI
455 considers about 32 reactive gases, whereas GC and GMI have over 100, and FOAM has
456 more than 600. The other major difference across models is photolysis, with models
457 having different cloud data and different methods for calculating photolysis rates in
458 cloudy atmospheres (H2018). The three central models (GC, GMI, UCI) in terms of their
459 5 d variability (Table S9) are also most closely alike in these statistics with rms = 20 %–
460 30 % for L-CH₄ up to 26 %–35 % for P-O₃. These rms values appear to be about as
461 close as any two models can get. The intra-model rms for different years (UCI 2016
462 versus 1997) is 10 %–13 % and shows that we are seeing basic differences in the
463 chemical models across GC, GMI, and UCI. FOAM is the next closest to these central
464 models, but it will inherently have a larger rms because it is a 1 d calculation and not a 5
465 d average. NCAR's rms is consistently higher and likely related to what is seen in the 5 d
466 σ values in Table S9. GISS is clearly different from all the others (L-CH₄ rms > 100 %
467 while L-O₃ rms < 66 %).

468

469 **4 Results**

470

471 Our analysis of the reactivities uses the six-model RDS-0 results to examine the
472 consistency in calculating the Rs across models. Thereafter, we rely on the similar results
473 from the three central models (GC, GMI, UCI) to justify use of UCI^Z* RDS*-2b-with
474 MDS-2b as our best estimate for ATom reactivities. The uncertainty in this estimate can
475 be approximated by the inter-model spread of the central models as discussed above.
476 When evaluating the model's climatologies for chemical species, we use MDS-2b. A
477 summary of the key data files used here, as well as their sources and contents, is given in
478 Table 4.

479

480 **4.1 Probability densities of the reactivities**

481

482 The reactivities for three large domains (Global, Pacific, Atlantic) from the six-model
483 RDS-0 are summarized in Tables 2 and S8. Sorted PDs for the three Rs and Pacific and
484 Atlantic Ocean basins are plotted in Fig. 1 and show the importance of the most reactive
485 “hot” parcels with deeply convex curves and the sharp upturn in R values above 0.9
486 cumulative weight (top 10 %). Both basins show a similar emphasis on the most reactive
487 hot parcels: 80 % – 90 % of total R is in the top 50 % of the parcels, 25 % – 35 % is in
488 the top 10 %, and about 10 % – 14 % is in the top 3 %. The corollary is that the bottom
489 50 % parcels control only 10 % – 20 % of the total reactivity, which is why the median is
490 less than mean (except for P-O₃ in the Atlantic).

491

492 The enhancement factor for the top 50 % L-CH₄ parcels is 2.0 (84 % of reactivity in 42
493 % of mass) given that our 53 °S – 60 °N transects cover 83 % of the air mass below 200
494 hPa and assuming that L-CH₄ is negligible poleward of these transects. This
495 enhancement factor is a large-scale feature because the tropical lower troposphere, being

496 warm and wet with high sun, dominates the budget. It is seen in previous model
497 intercomparisons that calculate budgets in large tropospheric blocks like Voulgarakis et
498 al. (2013) with 63 % of L-CH₄ in 31 % of the air mass (500 hPa–surface, 30 °S – 30 °N).
499 The impact of the extremely hot parcels and the heterogeneity seen in the ATom 10 s
500 parcels is evident in the steep slopes above the 90th percentile, yielding enhancement
501 factors of 3 to 4.

502
503 Each R value and each ocean has a unique shape; for example L-O₃ in the Atlantic is
504 almost two straight lines breaking at the 50th percentile. In Fig. 1 the agreement across
505 all models (except GISS) is clear, indicating that the conclusion in *P2018* (i.e., that most
506 global chemistry models agree on the O₃ and CH₄ budgets if given the chemical
507 composition) also holds for the ATom-measured chemical composition. Comparing the
508 brown (UCI, RDS-0) and black-dashed (UCIZ, RDS*-2) lines, we find that the shift from
509 MDS-0 to MDS-2b plus the new RDS* (HNO₄+PAN) protocol produces large reductions
510 in P-O₃ for all cumulative weights and small reductions in L-CH₄ for the upper 5th
511 percentile. We conclude that accurate modeling of chemical composition of the 80th and
512 greater percentiles is important but that modest errors in the lowest 50th percentile are
513 inconsequential; effectively, some parcels matter more than others (P2017).

514
515 How well does this ATom analysis work as a model intercomparison project? Overall,
516 we find that most models give similar results when presented with the ATom-1 MDS.
517 The broad agreement of the cumulative reactive PDs across a range of model
518 formulations using differing levels of chemical complexity shows this approach is robust.
519 The different protocols for calculating reactivities as well as the uncertainty in cloud
520 fields appear to have a small impact on the shape of the cumulative PDs but are
521 informative regarding the minimum structural uncertainty in estimating the 24 h
522 reactivity of a well-measured air parcel.

523 4.2 Spatial heterogeneity of tropospheric chemistry

524 A critical unknown for tropospheric chemistry modeling is what resolution is needed to
525 correctly calculate the budgets of key gases. A similar question was addressed in Yu et
526 al. (2016) for the isoprene oxidation pathways using a model with variable resolution
527 (500 km, 250 km and 30 km) compared to aircraft measurements; see also ship plume
528 chemistry in Charlton-Perez et al. (2009). ATom's 10 s air parcels measure 2 km
529 (horizontal) by 80 m (vertical) during most profiles. There are obviously some chemical
530 structures below the 10 s air parcels ~~we use here~~. Only some ATom measurements are
531 archived at 1 Hz, and we examine a test case using 1 s data for O₃ and H₂O for a mid-
532 ocean descent between Anchorage and Kona in Fig. S2a in the Supplement. Some of the
533 1 s (200 m by 8 m) variability is clearly lost with 10 s averaging, but 10 s averaging
534 preserves most of the variability. Lines in Fig. S2 demark 400 m in altitude, and most of
535 the variability ~~appears to occur~~ on this larger, model-resolved scale. Fig. S2b shows the
536 10 s reactivities during that descent and also indicates that much of the variability occurs
537 at 400 m vertical scales. A more quantitative example using all the tropical ATom
538 reactivities is shown in comparisons with probability densities below (Fig. 5).

539 How important is it for the models to represent the extremes of reactivity? While the
540 sorted reactivity curves (Fig. 1, Tables 2 & S8) continue to steepen from the 90th to 97th
541 percentile, the slope does not change that much. Thus we can estimate the 99th+
542 percentile contributes <5% of the total reactivity. Thus, if our model misses the top 1 %
543 of reactive air parcels (e.g., due to the inability to simulate intensely reactive thin
544 pollution layers) then we miss at most 5 % of the total reactivity. This finding is new and
545 encouraging, and it needs to be verified with the ATom-2, 3, and 4 data.

546 The spatial structures and variability of reactivity as sampled by the ATom tropical
547 transects (central Pacific, eastern Pacific and Atlantic) are presented as nine panels in Fig.
548 2. Here, the UCIZ RDS*-2 reactivities are averaged and plotted in 1° latitude by 200 m
549 thick cells, comparable to some global models (e.g., GMI, NCAR, UCI). We separate the
550 eastern Pacific (121° W, research flight (RF) 1) from the Central Pacific (RFs 3, 4 and 5)
551 because we are looking for contiguous latitude-by-pressure structures.

552 In the central Pacific ([Fig. 2adgrow-1](#)), highly reactive (hot) P-O3 parcels (> 6 ppb/d)
553 occur in larger, connected air masses at latitudes 20°–22°N and pressure altitudes 2-3 km
554 and in more scattered parcels (> 3 ppb/d) below 5 km down to 20°S. High L-O3 and L-
555 CH4 coincide with this 20°–22°N air mass and also with some high P-O3 at lower
556 latitudes. This pattern of overlapping extremes in all three Rs is surprising because the
557 models' mid-Pacific climatologies show a separation between regions of high L-O3
558 (lower-middle troposphere) and high P-O3 (upper troposphere, as seen in P2017's Fig. 3).
559 The obvious explanation is that the models leave most of the lightning-produced NOx in
560 the upper troposphere. The ATom profiling seems to catch reactive regions in adjacent
561 profiles separate by a few hundred kilometers, scales easily resolvable with 3D models.

562 In the eastern Pacific ([Fig. 2behrow-2](#)), the overlap of outbound and return profiles
563 enhances the spatial sampling over the 10 h flight. The region of very large L-O3 (> 5
564 ppb/d) is extensive, beginning at 5–6 km at 10°N and broadening to 2–8 km at 28°N.
565 The region of L-CH4 is similar, but loss at the upper altitudes of this air mass is
566 attenuated because of the temperature dependence of L-CH4 and possibly because of
567 differing OH:HO₂ ratios with altitude. Large P-O3 (> 3 ppb/day) occurs only in the
568 center of this highly reactive L-O3/L-CH4 region, suggesting that NOx is not as evenly
569 distributed as is HOx. Highly reactive (hot) P-O3 parcels (> 4 ppb/day) occur only in the
570 upper troposphere (8–12 km) and only in the sub-tropics. ATom-1 RF1 (29 Jul 2016)
571 occurred during the North American Monsoon when there was easterly flow off Mexico,
572 thus the high reactivity of this large air mass indicates that continental deep convection
573 with lightning NOx is a source of high reactivity for both O₃ and CH₄.

574 In the Atlantic ([row-3Fig. 2cfi](#)) we also see similar air masses through successive profiles,
575 particularly in the northern tropics. The Atlantic P-O3 shows high-altitude reactivity
576 similar to the eastern Pacific. Likewise, the large values of L-O3 and L-CH4 match the
577 eastern Pacific and not central Pacific. Unlike either Pacific transect, the Atlantic L-O3
578 and L-CH4 show some high reactivity below 1 km altitude. Overall, the ATom-1
579 profiling clearly identifies extended air masses of high L-O3 and L-CH4 extending over
580 2–5 km in altitude and 10° of latitude. The high P-O3 regions tend to be much more
581 heterogeneous with greatly reduced spatial extent, likely of recent convective origin as
582 for eastern Pacific.

583 Overall, the extensive ATom profiling identifies a heterogeneous mix of chemical
584 composition in the tropical Atlantic and Pacific, with a large range of reactivities. What
585 is important for those trying to model tropospheric chemistry is that the spatial scales of
586 variability seen in Fig. 2 ~~should be are~~-within the capability of modern global models.

587 4.3 Testing model climatologies

588 The ATom data set provides a unique opportunity to test CTMs and CCMs in a
589 climatological sense. In this section, we compare ATom-1 data and the six models'
590 chemical statistics for mid-August used in P2017. The ATom profiles cannot be easily
591 compared point by point with CCMs, and we use statistical measures of the three
592 reactivities in the three tropical basins: mean profiles in Fig. 3 and PDs in Fig. 5.

593 4.3.1 Profiles

594 For P-O₃ profiles (top row, Fig. 3), the agreement between models and measurements is
595 passable except for the 0–2 km region in both Central and Eastern Pacific, where the
596 models fail to predict the observed 2 ppb/d O₃ production. In the Central Pacific at 3–12
597 km, ATom-1 results agree with models, showing ozone production of about 1 ppb/day.
598 In the Eastern Pacific and Atlantic at 3–12 km, ATom-1 results also agree with models,
599 but at a higher ozone production of about 2 ppb/day. This pattern indicates that in the
600 Central Pacific, the NO_x+HO_x combination that produces ozone is suppressed below 2
601 km in all the models. In the upper troposphere, 10–12 km, of the Eastern Pacific and
602 Atlantic, ATom P-O₃ values show a jump to 3 ppb/d, which is only partly reproduced in
603 the models. We take this pattern as evidence for lightning NO_x production and export
604 over the adjacent continents.

605 For L-O₃ (middle row, Fig. 3) in the central Pacific, ATom-1 results match the
606 throughout the 0–12 km range (except GISS). Moving to the eastern Pacific and Atlantic,
607 most models show a mid-level peak above 2 km, while ATom-1 shows even larger peak
608 L-O₃, especially in the Eastern Pacific at 3–6 km where L-O₃ > 4 ppb/d. This mid-
609 tropospheric peak is evident in the curtain plots of Fig. 2 and likely due to easterly mid-
610 tropospheric flow from convection over Mexico at that specific time (29 July 2016).
611 Similarly, the ATom reactivity at 1–3 km in the Atlantic is associated with biomass
612 burning in Africa and was measured in other trace species. Thus, in terms of L-O₃, the
613 ATom–model differences may be due to specific meteorological conditions, and this
614 could be tested with CTMs using 2016 meteorology and wildfires.

615
616 For L-CH₄ (bottom row, Fig. 3), the ATom-model patterns are similar to L-O₃, including
617 the large ATom-only losses (> 1.5 ppb/d over 3–6 km) in the eastern Pacific, but with
618 higher reactivities occurring at slightly lower altitudes because of the large negative
619 temperature dependence of reaction (1). L-O₃ is dominated by O(1D) and HO₂ loss,
620 while L-CH₄ is limited to OH loss. Overall, there is clear evidence that the Atlantic and
621 Pacific have very different chemical mixtures controlling the reactivities and that
622 convection over land (monsoon or biomass burning) creates air masses that are still
623 highly reactive a day or so later.

624 625 4.3.2 Key species

626 The deficit in modeled P-O₃ in the central and eastern Pacific at 0–2 km altitude points to
627 a NO_x deficiency in the models, and this becomes obvious in the comparison of the PD
628 histograms for NO_x shown in Fig. 4. Over 0–12 km (first row), ATom has a reduced
629 frequency of parcels with 1–10 ppt and a corresponding increase in parcels with 20–60
630 ppt; this discrepancy is amplified in the lower troposphere, 0–4 km (second row). The
631 **only**-obvious source of this oceanic NO_x is lightning since oceanic sources of
632 organonitrates or other nitrate species measured on ATom could not supply this amount.
633 The ATom statistics indicate such a lightning source must be mixed down into the
634 boundary layer. In the eastern Pacific and Atlantic, the full troposphere PD more closely
635 matches the models, including bump in 100–300 ppt NO_x which is probably direct
636 outflow from very deep convection with lightning over the neighboring continents.
637 Overall, the models appear to be missing significant NO_x sources in all three regions
638 below 4 km.

639
640 In Fig. 4, we also look at the histograms for the key HO_x-related species HOOH (third
641 row) and HCHO (fourth row). For these species, the ATom–model agreement is
642 generally good. If anything, the models tend to have too much HOOH. ATom shows
643 systematically large occurrences of low HOOH (50–200 ppt, especially central Pacific)
644 indicating, perhaps, that convective or cloud scavenging of HOOH is more effective than
645 is modeled. HCHO shows reasonable agreement in the Atlantic, but in both central and
646 eastern Pacific, the modeled low end (< 40 ppt) is simply not seen in the ATom data.
647 Also, the models are missing a strong HCHO peak at 300 ppt in the eastern Pacific,
648 probably convection-related **specific to that time period**. Thus, in terms of these HO_x
649 precursors, the model climatologies appear to be at least as reactive as the ATom data.

650 While the ATom-1 data in Fig. 4 are limited to single transects, the model NO_x
651 discrepancies apply across the three tropical regions, and the simple chemical statistics
652 for these flights alone are probably enough to identify measurement-model discrepancies.
653 For the HO_x-related species, the models match the first-order statistics from ATom. In
654 terms of using ATom statistics as a model metric, it is encouraging that where **some**
655 individual models tend to deviate from their peers, they also deviate from the ATom-1
656 PDs.

657 4.3.3 Probability densities

658 Mean profiles do not reflect the heterogeneity seen in Fig. 2, and so we also examine the
659 PDs of the tropical reactivities (Fig. 5). The model PDs (colored lines connecting open
660 circles at the center of each bin) are calculated from the 1 d statistics for mid-August
661 (P2017) using the model blocks shown in Fig. S1. The model grid cells are weighted by
662 air mass and cosine(latitude) and limited to pressures greater than 200 hPa. The ATom
663 PDs (black lines connecting black open circles) are calculated from the 10 s data
664 weighted by (but not averaged over) the number of points in each 10° latitude by 200 hPa
665 pressure bin, and then also by cosine (latitude) to compare with the models. In addition,
666 a PD was calculated from the 1° by 200 m average grid-cell values in Fig. 2 (black Xs),
667 and this is also cosine(latitude)-weighted. To check if the high reactivities in the eastern
668 Pacific affected the whole Pacific PD, a separate PD using only central Pacific 10 s data
669 was calculated (gray lines connecting gray open circles). The mean reactivities (ppb/d)

670 from the models and ATom are given in the legend; note that the model values are based
671 on the August climatologies (P2017) and not the MDS-0 values in the table. The 'ATom'
672 legend values are the same as in Table 2. The PD binning is shown by the open circles,
673 and occurrences of off-scale reactivities are included in the last point.

674
675 For the Pacific (eastern + central, left columns, Fig. 5), the modeled PD climatologies are
676 similar for each of the reactivities (except GISS), and there is fairly good agreement with
677 the ATom-1 PDs. ~~P-O3.~~ For the Atlantic (right columns, Fig. 5), the models show a
678 larger spread presumably due to the differing influence of pollution from neighboring
679 continents. The ATom-1 Atlantic PDs also show slightly larger disagreement with the
680 models (e.g., the maximum in P-O3 at 1–2 ppb/d and minimum in L-O3 at 2–3 ppb/d)
681 and the notably higher frequency of hot spots with L-O3 > 5 ppb/d. The influence of the
682 extreme eastern Pacific reactivities are seen in the statistics generated from the central
683 Pacific values only in the mean values in the legend: the central Pacific alone (CPac,
684 gray circles), e.g., the mean value for L-O3 drops from 1.42 to 1.17 ppb/d. is always less
685 than the total Pacific (ATom), particularly for L-O3.

686
687 The ability to test a model's reactivity statistics with the ATom 10 s data is not obvious,
688 but the PDs based on 1° latitude by 200 m altitude cells (the black Xs) are remarkably
689 close to the PDs based on 2 km (horizontal) by 80 m (vertical) 10 s parcels. With the
690 coarser resolution, we see a slight shift of points from the ends of the PD to the middle as
691 expected, but we find once again, that the loss in high-frequency, below-model grid-cell
692 resolution is not great. Both ATom-derived PDs more closely resemble each other than
693 any model PD. Thus, current global chemistry models with resolutions of about 100 km
694 by 400 m should be able to capture much of the wide range of chemical heterogeneity in
695 the atmosphere, which for the oceanic transects is, we believe, adequately resolved by the
696 10 s ATom measurements. Perhaps more surprising, given the different mean profiles in
697 Fig. 3, is that the five model PDs in Fig. 5 look very much alike.

698

699 5 Discussion and path forward

700

701 5.1 Major findings

702

703 This paper opens a door for what the community can do with the ATom measurements
704 and the derived products. ATom's mix of key species allows us to calculate the reactivity
705 of the air parcels and hopefully may become standard for tropospheric chemistry
706 campaigns. We find that the reactivity of the troposphere with respect to O₃ and CH₄ is
707 dominated by a fraction of the air parcels but not by so small and infrequent a fraction as
708 to challenge the ability of current CTMs to simulate these observations and thus be used
709 to study the oxidation budgets. In comparing ATom results with modeled climatologies,
710 we find a clear systematic ATom-model discrepancy difference: models show a large
711 relative drop in —missing— O₃ production below 2 km over the tropical oceans but ATom
712 shows an increase (C.Pac.), no change (E.Pac.) or a much lesser drop (Atl.). ²lowermost
713 (0–2 km) troposphere— We and traced this result to the lack of NO_x at the 20–60 ppt
714 levels in the models below 4 km and believe it provides a clear challenge in modeling

715 ~~ozone.-The occurrence of the same error over the central and eastern Pacific as well as~~
716 ~~the Atlantic Oceans makes this a robust finding.~~

717 Building our chemical statistics (PDs) from the ATom 10 s air parcels on a scale of 2 km
718 by 80 m, we can identify the fundamental scales of spatial heterogeneity in tropospheric
719 chemistry. Although heterogeneity occurs at the finest scales (such as seen in some 1 s
720 observations) the majority of variability in terms of the O₃ and CH₄ budgets occurs across
721 scales larger than neighboring 2 km parcels. The PDs measured in ATom can be largely
722 captured by a global models' 100 km by 200 m grid cells in the lower troposphere. This
723 surprising result is evident by comparing the ATom 1D PDs – both species and
724 reactivities – with those from the models' climatologies (Fig. 5). These comparisons
725 show that the modeled PDs are consistent with the innate chemical heterogeneity of the
726 troposphere as measured by the 10 s parcels in ATom. A related conclusion for biomass
727 burning smoke particles is found by Schill et al. (2020), where most of the smoke appears
728 in the background rather than in pollution plumes, and therefore much of the variability
729 occurs on synoptic scales resolved by global models (see their Fig. 1 compared with Fig.
730 2 here).

731 5.2 Opportunities and lessons learned

732 As a quick look at the opportunities provided by the ATom data, we present an example
733 based on the Wolfe et al (2019) study, which used the F0AM model and semi-analytical
734 arguments to show that troposphere HCHO columns (measurable by satellite and ATom)
735 are related to OH columns (measured by ATom) and thus to CH₄ loss. Fig. 6 extends the
736 Wolfe et al study using the individual air parcels and plotting L-CH₄ (ppb/d) versus
737 HCHO (ppt) for the three tropical regions where most of the CH₄ loss occurs. The
738 relationship is linear but with a lot of scatter and has slopes ranging from 3.5 to 4.4 per
739 day over the three tropical regions; but for the largest reactivities (0-4 km, 1–3 ppb/d), L-
740 CH₄ is not so well correlated with HCHO.

741
742 As is usual with new model intercomparison projects, we have an opportunity to identify
743 model 'features' and identify errors. In the UCI model, an error in the lumped alkane
744 formulation (averaging alkanes C₃H₈ and higher) did not show up in P2018, where UCI
745 supplied all the species, but when the ATom data were used, the UCI model became an
746 outlier. Once found, this problem was readily fixed (hence the current UCIZ model
747 version). Inclusion of the F0AM model with its extensive hydrocarbon oxidation
748 mechanism provided an interesting contrast with the simpler chemistry in the global
749 CCM/CTMs. For a better comparison of the chemical mechanisms, we should have
750 F0AM use 5 d of photolysis fields from one of the CTMs. The anomalous GISS results
751 have been examined by a co-author, but no clear causes have been identified as of this
752 publication. The problem goes beyond just the implementation of the RDS protocol, as it
753 shows up in the model climatology (Fig. 4 & 5, also in P2017).

754 Decadal-scale shifts in the budgets of O₃ and CH₄ are likely to be evident through the
755 statistical patterns of the key species, rather than simply via average profiles. The
756 underlying design of ATom was to collect enough data to develop such a multivariate
757 chemical climatology. As a quick look across the four deployments, we show the joint
758 2D PDs on a logarithmic scale as in P2017 for HOOH versus NO_x in Fig. 7. The patterns

759 for the tropical central Pacific are quite similar for the four seasons of ATom
760 deployments, and the fitted ellipses are almost identical for ATom 2, 3 and 4. Thus, for
761 these species in the central Pacific, we believe that ATom provides a benchmark of the
762 2016-2018 chemical state, one that can be revisited with an aircraft mission in a decade to
763 detect changes in not only chemical composition but also reactivity.

764 ATom identifies which ‘highly reactive’ spatial or chemical environments could be
765 targeted in future campaigns for process studies or to provide a better link between
766 satellite observations and photochemical reactivity (e.g., E. Pacific mid-troposphere in
767 August, Fig. 2). The many corollary species measured by ATom (not directly involved in
768 CH₄ and O₃ chemistry) can provide clues to the origin or chemical processing of these
769 environments. We hope to engage a wider modeling community beyond the ATom
770 science team, as in H2018, in the calculation of photochemical processes, budgets, and
771 feedbacks based on all four ATom deployments.

772

773 *Data Availability.* The MDS-2b and RDS*-2b data for ATom 1, 2, 3 and 4 are presented
774 here as core ATom deliverables, and are now posted on the NASA ESPO ATom website
775 (<https://espo.nasa.gov/atom/content/ATom>). This publication marks the public release of
776 the reactivity calculations for ATom 2, 3 and 4, but we have not yet analyzed these data,
777 and thus users should be aware and report any anomalous features to the lead authors via
778 haog2@uci.edu and mprather@uci.edu. Details of the ATom mission and data sets are
779 found on the NASA mission website (<https://espo.nasa.gov/atom/content/ATom>) and at
780 the final archive at Oak Ridge National Laboratory (ORNL;
781 https://daac.ornl.gov/ATOM/guides/ATom_merge.html). The MATLAB scripts and data
782 sets used in the analysis here are posted on Dryad (<https://doi.org/10.7280/D1Q699>).

783 *Supplement.* The supplement related to this article is available online at:
784 <https://doi.org/10.5194/acp-21-13729-2021-supplement>.

785 *Author Contributions.* HG, CMF, SCW and MJP designed the research and performed
786 the data analysis. SAS, SDS, LE, FL, JL, AMF, GC, LTM and GW contributed original
787 atmospheric chemistry model results. GW, MK, JC, GD, JD, BCD, RC, KM, JP, TBR,
788 CT, TFH, DB, NJB, ECA, RSH, JE, EH and FM contributed original atmospheric
789 observations. HG, CMF and MJP wrote the paper.

790 *Competing interests.* The contact author has declared that neither they nor their co-
791 authors have any competing interests

792 *Acknowledgments.* The authors are indebted to the entire ATom Science Team including
793 the managers, pilots and crew, who made this mission possible. Many other scientists not
794 on the author list enabled the measurements and model results used here. [The authors](#)
795 [thank Ms. Xin Zhu for maintaining and updating the UCI Chemistry Transport Model](#)
796 [used here.](#)

797

798 *Financial support.* The Atmospheric Tomography Mission (ATom) was supported by the
799 National Aeronautics and Space Administration's Earth System Science Pathfinder

800 Venture-Class Science Investigations: Earth Venture Suborbital-2. Primary funding of the
801 preparation of this paper at UC Irvine was through NASA (grant nos. NNX15AG57A and
802 80NSSC21K1454).

803

804 *Review statement.* This paper was edited by Neil Harris and reviewed by two anonymous
805 referees.

806

807 **References**

- 808 Burkholder, J. B., Sander, S. P., Abbatt, J. P. D., Barker, J. R., Huie, R. E., Kolb, C. E.,
809 Kurylo, M. J., Orkin, V. L., Wilmouth, D. M., and Wine, P. H.: Chemical kinetics and
810 photochemical data for use in atmospheric studies: evaluation number 18, Pasadena, CA,
811 Jet Propulsion Laboratory, National Aeronautics and Space Administration, available at:
812 <http://hdl.handle.net/2014/45510> (last access: 13 September 2021), 2015.
- 813 Charlton-Perez, C. L., Evans, M. J., Marsham, J. H., and Esler, J. G.: The impact of
814 resolution on ship plume simulations with NO_x chemistry, *Atmos. Chem. Phys.*, 9, 7505–
815 7518, <https://doi.org/10.5194/acp-9-7505-2009>, 2009.
- 816 Douglass, A. R., Prather, M. J., Hall, T. M., Strahan, S. E., Rasch, P. J., Sparling, L. C.,
817 Coy, L., and Rodriguez, J. M.: Choosing meteorological input for the global modeling
818 initiative assessment of high-speed aircraft, *J. Geophys. Res.-Atmos.*, 104, 27545–27564,
819 <https://doi.org/10.1029/1999JD900827>, 1999.
- 820 Eastham, S. D. and Jacob, D. J.: Limits on the ability of global Eulerian models to resolve
821 intercontinental transport of chemical plumes, *Atmos. Chem. Phys.*, 17, 2543–2553,
822 <https://doi.org/10.5194/acp-17-2543-2017>, 2017.
- 823 Griffiths, P. T., Murray, L. T., Zeng, G., Shin, Y. M., Abraham, N. L., Archibald, A. T.,
824 Deushi, M., Emmons, L. K., Galbally, I. E., Hassler, B., Horowitz, L. W., Keeble, J., Liu,
825 J., Moeini, O., Naik, V., O'Connor, F. M., Oshima, N., Tarasick, D., Tilmes, S., Turnock,
826 S. T., Wild, O., Young, P. J., and Zanis, P.: Tropospheric ozone in CMIP6 simulations,
827 *Atmos. Chem. Phys.*, 21, 4187–4218, <https://doi.org/10.5194/acp-21-4187-2021>, 2021.
- 828 Guo, H.: Heterogeneity and chemical reactivity of the remote Troposphere defined by
829 aircraft measurements, Dryad [data set], <https://doi.org/10.7280/D1Q699>, 2021.
- 830 Hall, S. R., Ullmann, K., Prather, M. J., Flynn, C. M., Murray, L. T., Fiore, A. M.,
831 Correa, G., Strode, S. A., Steenrod, S. D., Lamarque, J.-F., Guth, J., Josse, B., Flemming,
832 J., Huijnen, V., Abraham, N. L., and Archibald, A. T.: Cloud impacts on photochemistry:
833 building a climatology of photolysis rates from the Atmospheric Tomography mission,
834 *Atmos. Chem. Phys.*, 18, 16809–16828, <https://doi.org/10.5194/acp-18-16809-2018>,
835 2018.
- 836 Heald, C. L., Coe, H., Jimenez, J. L., Weber, R. J., Bahreini, R., Middlebrook, A. M.,
837 Russell, L. M., Jolleys, M., Fu, T.-M., Allan, J. D., Bower, K. N., Capes, G., Crosier, J.,
838 Morgan, W. T., Robinson, N. H., Williams, P. I., Cubison, M. J., DeCarlo, P. F., and
839 Dunlea, E. J.: Exploring the vertical profile of atmospheric organic aerosol: comparing 17
840 aircraft field campaigns with a global model, *Atmos. Chem. Phys.*, 11, 12673–12696,
841 <https://doi.org/10.5194/acp-11-12673-2011>, 2011.
- 842 Myhre, G., Shindell, D., and Pongratz, J.: Anthropogenic and Natural Radiative Forcing,
843 in *Climate Change 2013: The Physical Science Basis*, IPCC WGI Contribution to the

844 Fifth Assessment Report, Cambridge University Press, 659–740,
845 <https://doi.org/10.1017/CBO9781107415324.018>, 2014.

846 Naik, V., Voulgarakis, A., Fiore, A. M., Horowitz, L. W., Lamarque, J.-F., Lin, M.,
847 Prather, M. J., Young, P. J., Bergmann, D., Cameron-Smith, P. J., Cionni, I., Collins, W.
848 J., Dalsøren, S. B., Doherty, R., Eyring, V., Faluvegi, G., Folberth, G. A., Josse, B., Lee,
849 Y. H., MacKenzie, I. A., Nagashima, T., van Noije, T. P. C., Plummer, D. A., Righi, M.,
850 Rumbold, S. T., Skeie, R., Shindell, D. T., Stevenson, D. S., Strode, S., Sudo, K., Szopa,
851 S., and Zeng, G.: Preindustrial to present-day changes in tropospheric hydroxyl radical
852 and methane lifetime from the Atmospheric Chemistry and Climate Model
853 Intercomparison Project (ACCMIP), *Atmos. Chem. Phys.*, 13, 5277–5298,
854 <https://doi.org/10.5194/acp-13-5277-2013>, 2013.

855 Prather, M. J., Ehhalt, D., Dentener, F., Derwent, R., Dlugokencky, E. J., Holland, E.,
856 Isaksen, I., Katima, J., Kirchhoff, V., Matson, P., and Midgley, P.: Chapter 4 –
857 Atmospheric Chemistry and Greenhouse Gases, *Climate Change 2001: The Scientific*
858 *Basis, Third Assessment Report of the Intergovernmental Panel on Climate Change*, 239–
859 287, 2001.

860 Prather, M. J., Zhu, X., Flynn, C. M., Strode, S. A., Rodriguez, J. M., Steenrod, S. D.,
861 Liu, J., Lamarque, J.-F., Fiore, A. M., Horowitz, L. W., Mao, J., Murray, L. T., Shindell,
862 D. T., and Wofsy, S. C.: Global atmospheric chemistry – which air matters, *Atmos.*
863 *Chem. Phys.*, 17, 9081–9102, <https://doi.org/10.5194/acp-17-9081-2017>, 2017.

864 Prather, M. J., Flynn, C. M., Zhu, X., Steenrod, S. D., Strode, S. A., Fiore, A. M., Correa,
865 G., Murray, L. T., and Lamarque, J.-F.: How well can global chemistry models calculate
866 the reactivity of short-lived greenhouse gases in the remote troposphere, knowing the
867 chemical composition, *Atmos. Meas. Tech.*, 11, 2653–2668, [https://doi.org/10.5194/amt-](https://doi.org/10.5194/amt-11-2653-2018)
868 [11-2653-2018](https://doi.org/10.5194/amt-11-2653-2018), 2018.

869 Rastigejev, Y., Park, R., Brenner, M. P., and Jacob, D. J.: Resolving intercontinental
870 pollution plumes in global models of atmospheric transport, *J. Geophys. Res.-Atmos.*,
871 115, D012568, <https://doi.org/10.1029/2009JD012568>, 2010.

872 Schill, G. P., Froyd, K. D., Bian, H., Kupc, A., Williamson, C., Brock, C. A., Ray, E.,
873 Hornbrook, R. S., Hills, A. J., Apel, E. C., and Chin, M.: Widespread biomass burning
874 smoke throughout the remote troposphere, *Nat. Geosci.*, 13, 422–427,
875 <https://doi.org/10.1038/s41561-020-0586-1>, 2020.

876 Science team of the NASA Atmospheric Tomography Mission: ATom [data set],
877 available at: <https://espo.nasa.gov/atom/content/ATom>, last access: 13 September 2021.

878 Stevenson, D. S., Dentener, F. J., Schultz, M. G., Ellingsen, K., Van Noije, T. P. C.,
879 Wild, O., Zeng, G., Amann, M., Atherton, C. S., Bell, N., and Bergmann, D. J.:
880 Multimodel ensemble simulations of present-day and near-future tropospheric ozone, *J.*
881 *Geophys. Res.-Atmos.*, 111, D006338, <https://doi.org/10.1029/2005JD006338>, 2006.

882 Stevenson, D. S., Young, P. J., Naik, V., Lamarque, J.-F., Shindell, D. T., Voulgarakis,
883 A., Skeie, R. B., Dalsoren, S. B., Myhre, G., Berntsen, T. K., Folberth, G. A., Rumbold,
884 S. T., Collins, W. J., MacKenzie, I. A., Doherty, R. M., Zeng, G., van Noije, T. P. C.,
885 Strunk, A., Bergmann, D., Cameron-Smith, P., Plummer, D. A., Strode, S. A., Horowitz,
886 L., Lee, Y. H., Szopa, S., Sudo, K., Nagashima, T., Josse, B., Cionni, I., Righi, M.,
887 Eyring, V., Conley, A., Bowman, K. W., Wild, O., and Archibald, A.: Tropospheric
888 ozone changes, radiative forcing and attribution to emissions in the Atmospheric
889 Chemistry and Climate Model Intercomparison Project (ACCMIP), *Atmos. Chem. Phys.*,
890 13, 3063–3085, <https://doi.org/10.5194/acp-13-3063-2013>, 2013.

891 Stevenson, D. S., Zhao, A., Naik, V., O'Connor, F. M., Tilmes, S., Zeng, G., Murray, L.
892 T., Collins, W. J., Griffiths, P. T., Shim, S., Horowitz, L. W., Sentman, L. T., and
893 Emmons, L.: Trends in global tropospheric hydroxyl radical and methane lifetime since
894 1850 from AerChemMIP, *Atmos. Chem. Phys.*, 20, 12905–12920,
895 <https://doi.org/10.5194/acp-20-12905-2020>, 2020.

896 Stocker, T. F., Qin, D., Plattner, G. K., Tignor, M., Allen, S. K., Boschung, J., Nauels, A.,
897 Xia, Y., Bex, V., and Midgley, P. M.: Contribution of working group I to the fifth
898 assessment report of the intergovernmental panel on climate change. Cambridge
899 University Press, 33–115, 2013.

900 Tie, X., Brasseur, G., and Ying, Z.: Impact of model resolution on chemical ozone
901 formation in Mexico City: application of the WRF-Chem model, *Atmos. Chem. Phys.*,
902 10, 8983–8995, <https://doi.org/10.5194/acp-10-8983-2010>, 2010.

903 Voulgarakis, A., Naik, V., Lamarque, J.-F., Shindell, D. T., Young, P. J., Prather, M. J.,
904 Wild, O., Field, R. D., Bergmann, D., Cameron-Smith, P., Cionni, I., Collins, W. J.,
905 Dalsøren, S. B., Doherty, R. M., Eyring, V., Faluvegi, G., Folberth, G. A., Horowitz, L.
906 W., Josse, B., MacKenzie, I. A., Nagashima, T., Plummer, D. A., Righi, M., Rumbold, S.
907 T., Stevenson, D. S., Strode, S. A., Sudo, K., Szopa, S., and Zeng, G.: Analysis of present
908 day and future OH and methane lifetime in the ACCMIP simulations, *Atmos. Chem.*
909 *Phys.*, 13, 2563–2587, <https://doi.org/10.5194/acp-13-2563-2013>, 2013.

910 Wofsy, S. C.: HIAPER Pole-to-Pole Observations (HIPPO): fine-grained, global-scale
911 measurements of climatically important atmospheric gases and aerosols, *Philos. T. R.*
912 *Soc. A*, 369, 2073–2086, <https://doi.org/10.1098/rsta.2010.0313>, 2011.

913 Wofsy, S. C., Afshar, S., Allen, H. M., Apel, E. C., Asher, E. C., Barletta, B., Bent, J.,
914 Bian, H., Biggs, B. C., Blake, D. R., Blake, N., Bourgeois, I., Brock, C. A., Brune, W. H.,
915 Budney, J. W., Bui, T. P., Butler, A., Campuzano-Jost, P., Chang, C.S., Chin, M.,
916 Commane, R., Correa, G., Crouse, J. D., Cullis, P. D., Daube, B.C., Day, D. A., Dean-
917 Day, J. M., Dibb, J. E., DiGangi, J. P., Diskin, G. S., Dollner, M., Elkins, J. W., Erdesz,
918 F., Fiore, A. M., Flynn, C. M., Froyd, K. D., Gesler, D. W., Hall, S. R., Hanisco, T. F.,
919 Hannun, R. A., Hills, A. J., Hints, E. J., Hoffman, A., Hornbrook, R. S., Huey, L. G.,
920 Hughes, S., Jimenez, J. L., Johnson, B. J., Katich, J. M., Keeling, R. F., Kim, M. J.,
921 Kupc, A., Lait, L. R., Lamarque, J.-F., Liu, J., McKain, K., Mclaughlin, R. J., Meinardi,

922 S., Miller, D. O., Montzka, S. A., Moore, F. L., Morgan, E. J., Murphy, D. M., Murray, L.
923 T., Nault, B. A., Neuman, J. A., Newman, P. A., Nicely, J. M., Pan, X., Paplawsky, W.,
924 Peischl, J., Prather, M. J., Price, D. J., Ray, E. A., Reeves, J. M., Richardson, M., Rollins,
925 A. W., Rosenlof, K. H., Ryerson, T. B., Scheuer, E., Schill, G. P., Schroder, J. C.,
926 Schwarz, J. P., St.Clair, J. M., Steenrod, S. D., Stephens, B. B., Strode, S. A., Sweeney,
927 C., Tanner, D., Teng, A. P., Thames, A. B., Thompson, C. R., Ullmann, K., Veres, P. R.,
928 Vieznor, N., Wagner, N. L., Watt, A., Weber, R., Weinzierl, B., Wennberg, P. O.,
929 Williamson, C. J., Wilson, J. C., Wolfe, G. M., Woods, C. T., and Zeng L. H.: ATom:
930 Merged Atmospheric Chemistry, Trace Gases, and Aerosols, ORNL DAAC [data set],
931 Oak Ridge, Tennessee, USA, <https://doi.org/10.3334/ORNLDAAC/1581>, 2018.

932 Wolfe, G. M., Nicely, J. M., Clair, J. M. S., Hanisco, T. F., Liao, J., Oman, L. D., Brune,
933 W. B., Miller, D., Thames, A., Abad, G. G., and Ryerson, T. B.: Mapping hydroxyl
934 variability throughout the global remote troposphere via synthesis of airborne and
935 satellite formaldehyde observations, *P. Natl. Acad. Sci. USA*, 116, 11171–11180,
936 <https://doi.org/10.1073/pnas.1821661116>, 2019.

937 Young, P. J., Archibald, A. T., Bowman, K. W., Lamarque, J.-F., Naik, V., Stevenson, D.
938 S., Tilmes, S., Voulgarakis, A., Wild, O., Bergmann, D., Cameron-Smith, P., Cionni, I.,
939 Collins, W. J., Dalsøren, S. B., Doherty, R. M., Eyring, V., Faluvegi, G., Horowitz, L.
940 W., Josse, B., Lee, Y. H., MacKenzie, I. A., Nagashima, T., Plummer, D. A., Righi, M.,
941 Rumbold, S. T., Skeie, R. B., Shindell, D. T., Strode, S. A., Sudo, K., Szopa, S., and
942 Zeng, G.: Pre-industrial to end 21st century projections of tropospheric ozone from the
943 Atmospheric Chemistry and Climate Model Intercomparison Project (ACCMIP), *Atmos.*
944 *Chem. Phys.*, 13, 2063–2090, <https://doi.org/10.5194/acp-13-2063-2013>, 2013.

945 Young, P. J., Naik, V., Fiore, A. M., Gaudel, A., Guo, J., Lin, M. Y., Neu, J. L., Parrish,
946 D. D., Rieder, H. E., Schnell, J. L., and Tilmes, S.: Tropospheric Ozone Assessment
947 Report: Assessment of global-scale model performance for global and regional ozone
948 distributions, variability, and trends, *Elementa*, 6, 10,
949 <https://doi.org/10.1525/elementa.265>, 2018.

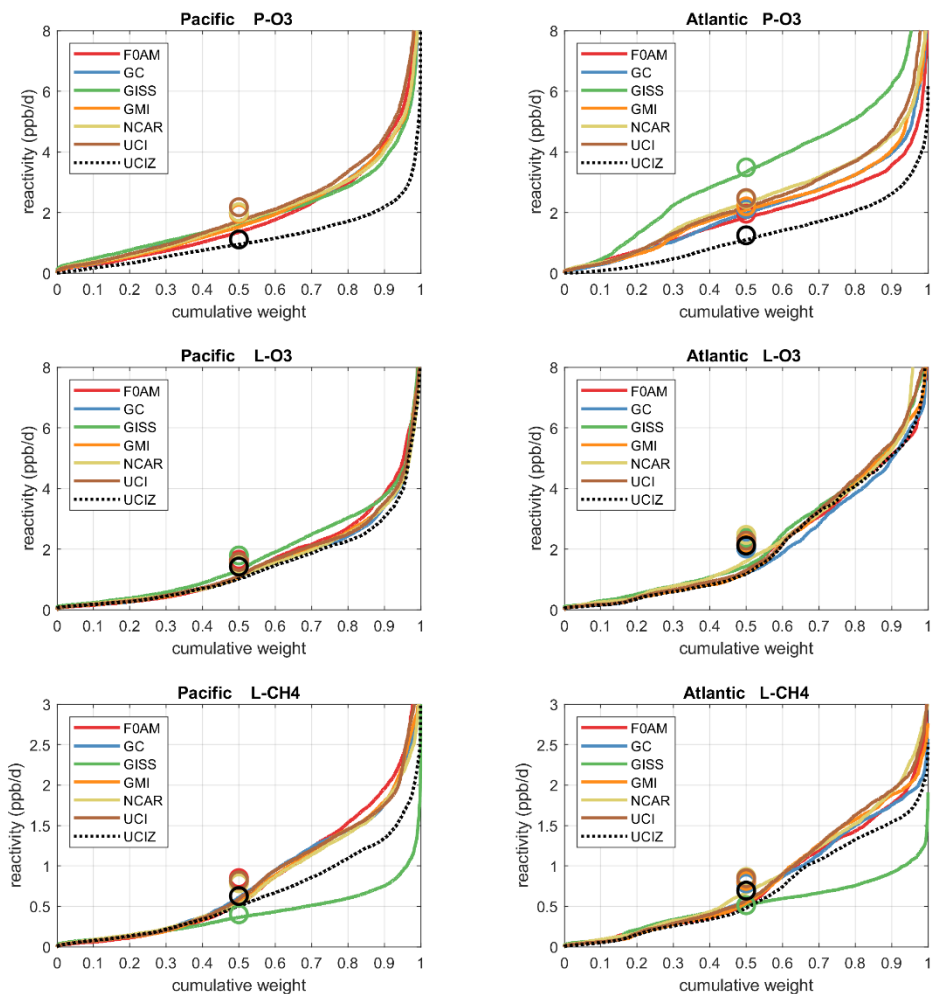
950 Yu, K., Jacob, D. J., Fisher, J. A., Kim, P. S., Marais, E. A., Miller, C. C., Travis, K. R.,
951 Zhu, L., Yantosca, R. M., Sulprizio, M. P., Cohen, R. C., Dibb, J. E., Fried, A.,
952 Mikoviny, T., Ryerson, T. B., Wennberg, P. O., and Wisthaler, A.: Sensitivity to grid
953 resolution in the ability of a chemical transport model to simulate observed oxidant
954 chemistry under high-isoprene conditions, *Atmos. Chem. Phys.*, 16, 4369–4378,
955 <https://doi.org/10.5194/acp-16-4369-2016>, 2016.

956 Zhuang, J., Jacob, D. J., and Eastham, S. D.: The importance of vertical resolution in the
957 free troposphere for modeling intercontinental plumes, *Atmos. Chem. Phys.*, 18, 6039–
958 6055, <https://doi.org/10.5194/acp-18-6039-2018>, 2018.

959

960
961

Figures and Tables



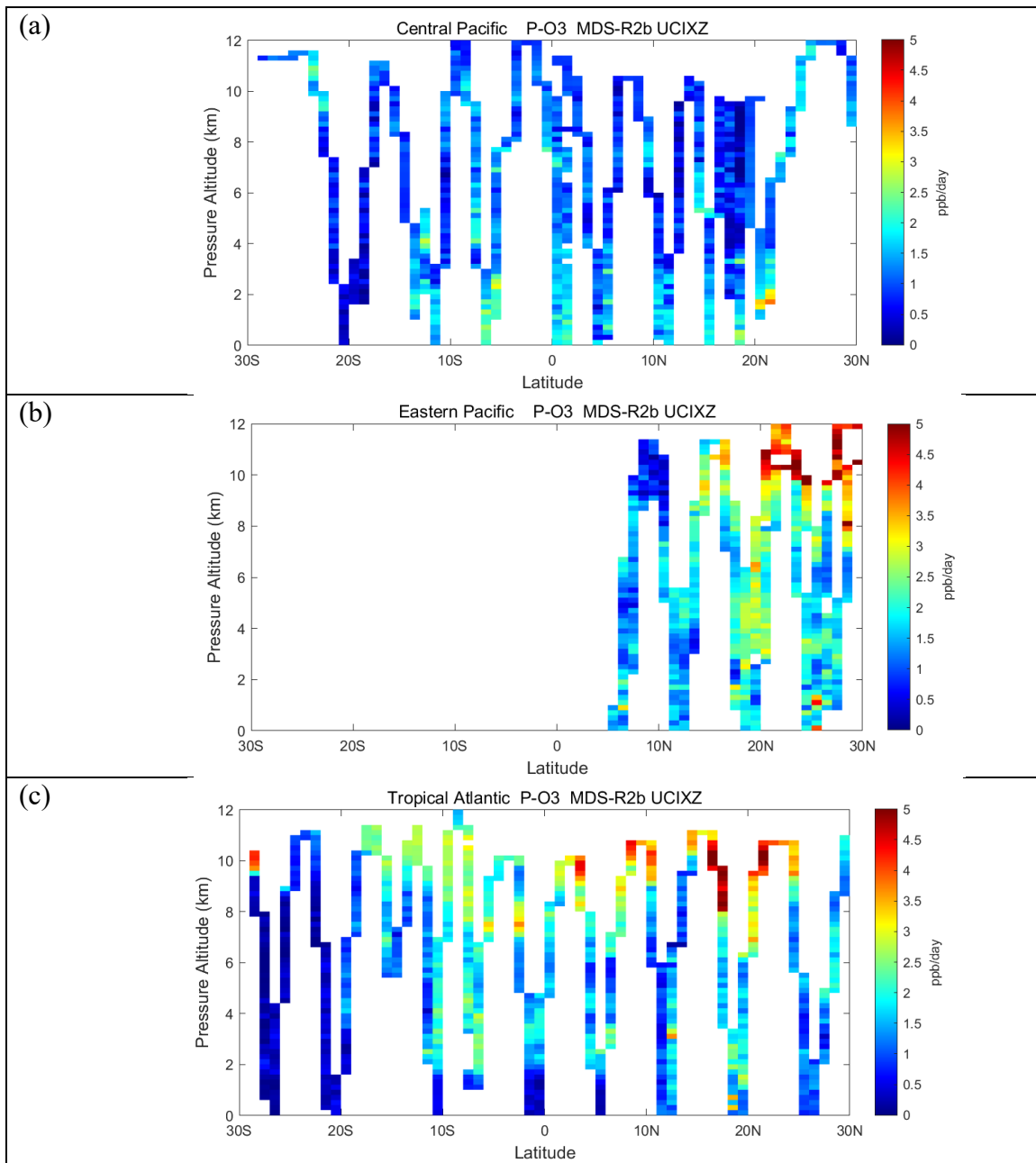
962

963

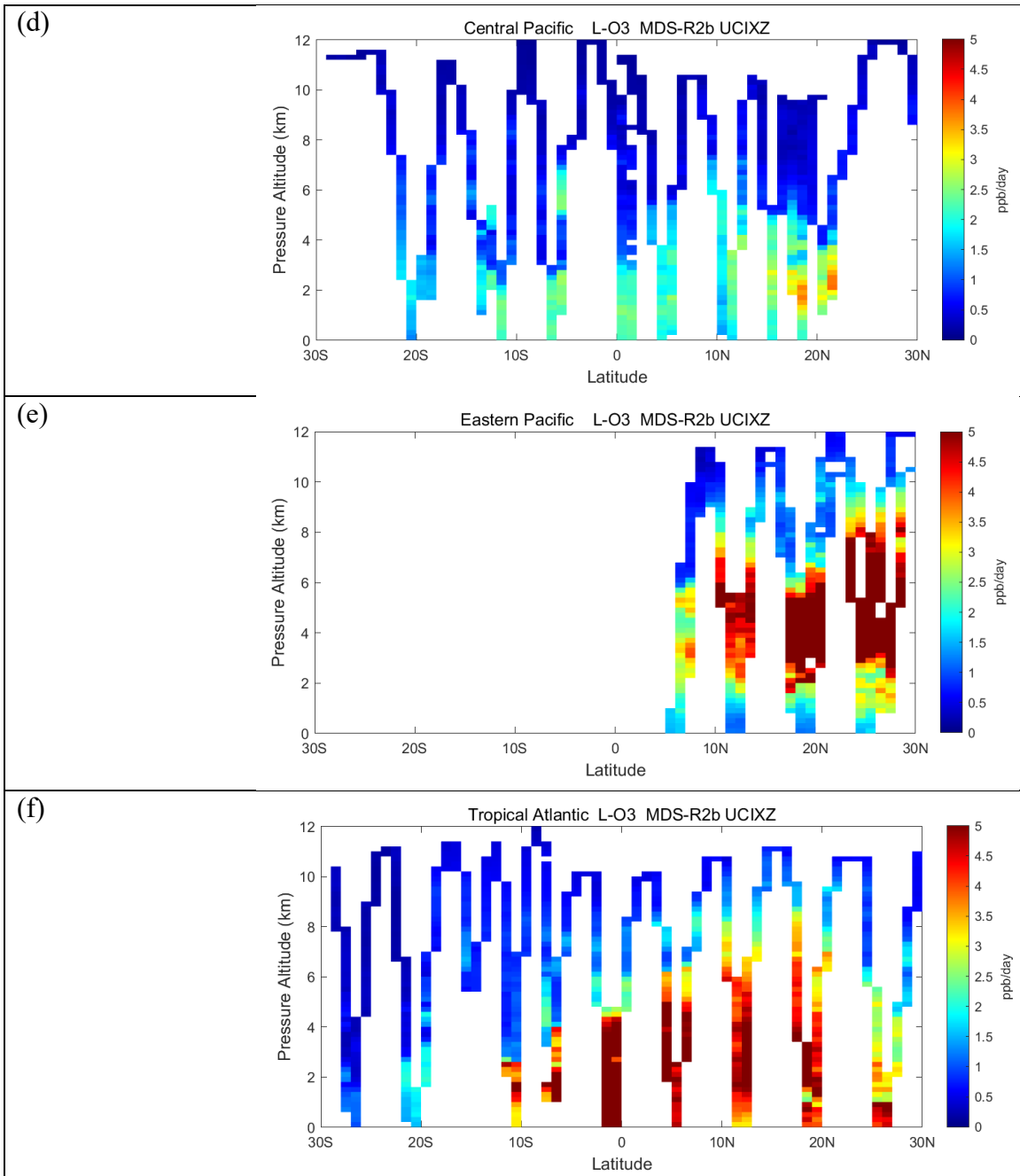
964 **Fig. 1** ~~Corr.~~ Sorted reactivities (P-O3, L-O3, L-CH4, ppb/day; three successive rows) for the
965 Pacific and Atlantic domains (53° S–60° N, two columns) of ATom-1. Each parcel is weighted,
966 including cosine(latitude), see text. ~~Results from The six models using ed reactivities for MDS-0~~
967 ~~model comparison using and~~ the standard RDS protocol are shown with colored lines; ~~and~~
968 ~~the updated corrected-UCIZ CTM calculation for using MDS-2b with the using the RDS*~~ protocol
969 (HNO₄ and PAN damping) is shown as a black dashed line. The mean value for each model is
970 shown with an open circle plotted at the 50th percentile. (Flipped about the axes, this is a
971 cumulative probability density function.)

972

973

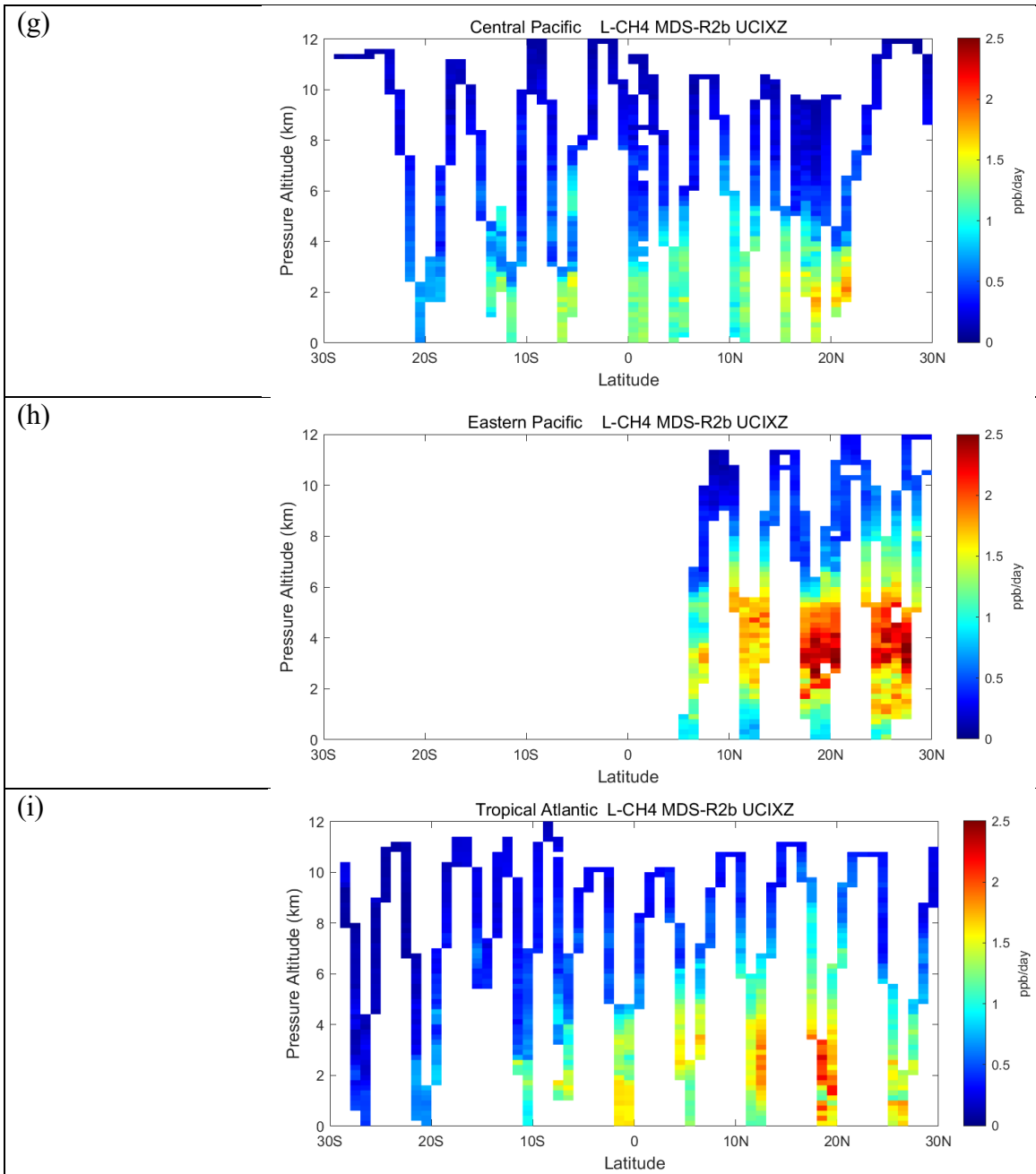


975 **Fig. 2abc.** Curtain plots for P-O3 (0–5 ppb/d; Fig 2abc), L-O3 (0–5 ppb/d; Fig 2def) and L-CH4
 976 (0–2.5 ppb/d; Fig 2ghi) showing the profiling of ATom-1 flights in the central Pacific (RF 3, 4
 977 and 5; Fig 2adg), eastern Pacific (RF 1; Fig2 beh), and Atlantic (RF 7, 8, and 9; Fig2cfi).
 978 Reactivities are calculated with the current UCIZ CTM model using MDS-2b and the RDS*
 979 protocol, see text. The 10 s air parcels are averaged into 1° latitude and 200 m altitude bins.
 980



981
982
983

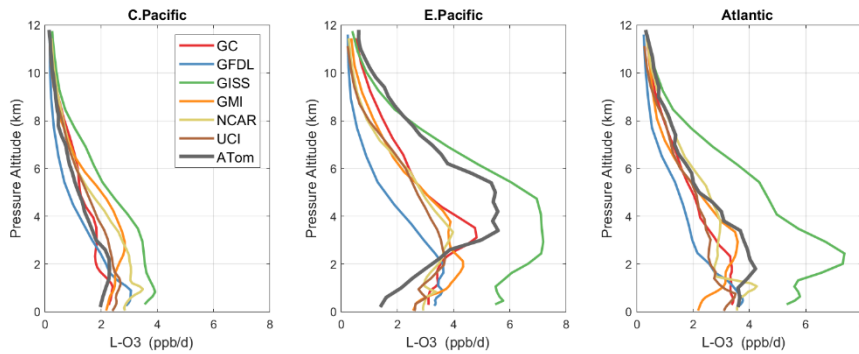
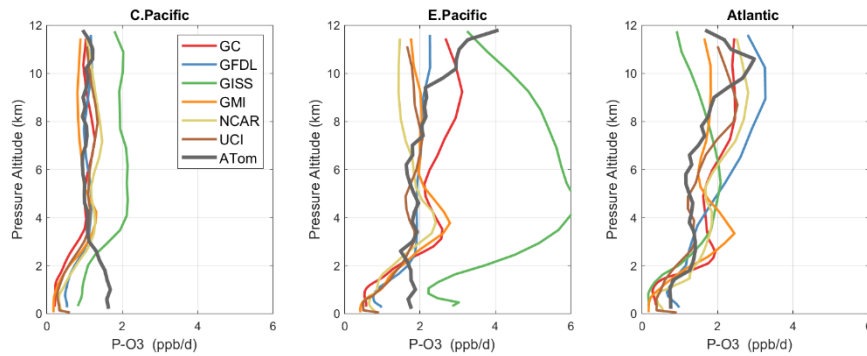
Fig. 2def.



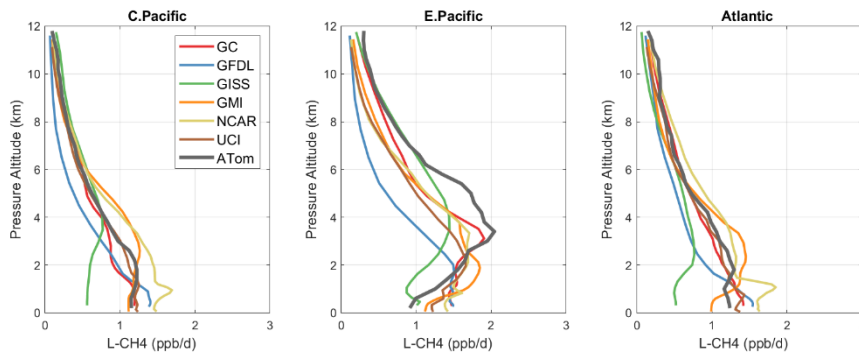
984
985
986

Fig. 2ghi.

987



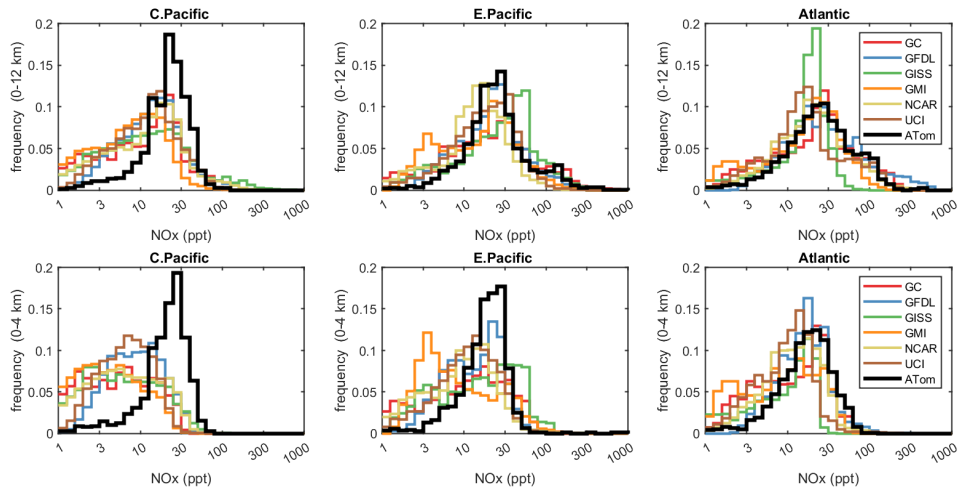
988



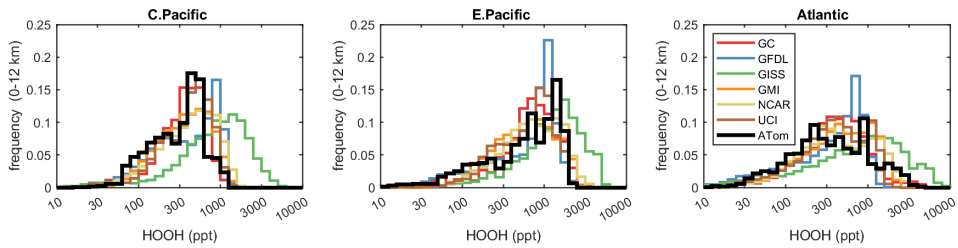
989

990 **Fig. 3** ~~Corr.~~ Mean altitude profiles of reactivity (rows: P-O3, L-O3, L-CH4 in ppb/day) in 3
991 domains (columns: C. Pacific, 30° S–30° N by 180°–210° E; E. Pacific, 0°–30° N by 230°–250°
992 E; Atlantic, 30° S–30° N by 326°–343° E; ranges are the model blocks). Air parcels are
993 cosine(latitude) weighted. ATom-1 (gray) results are from Fig. 2, while model results are taken
994 from the August climatologies in Prather et al. (2017).

995

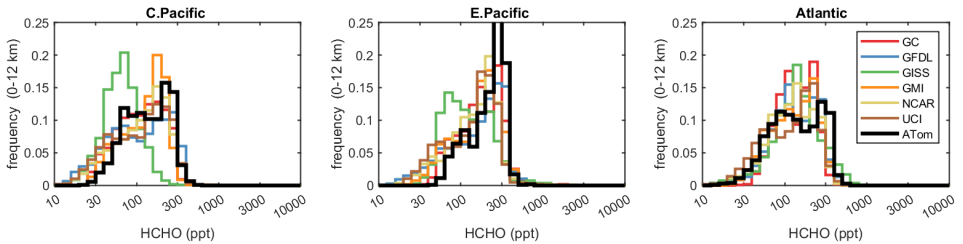


996
997



1005

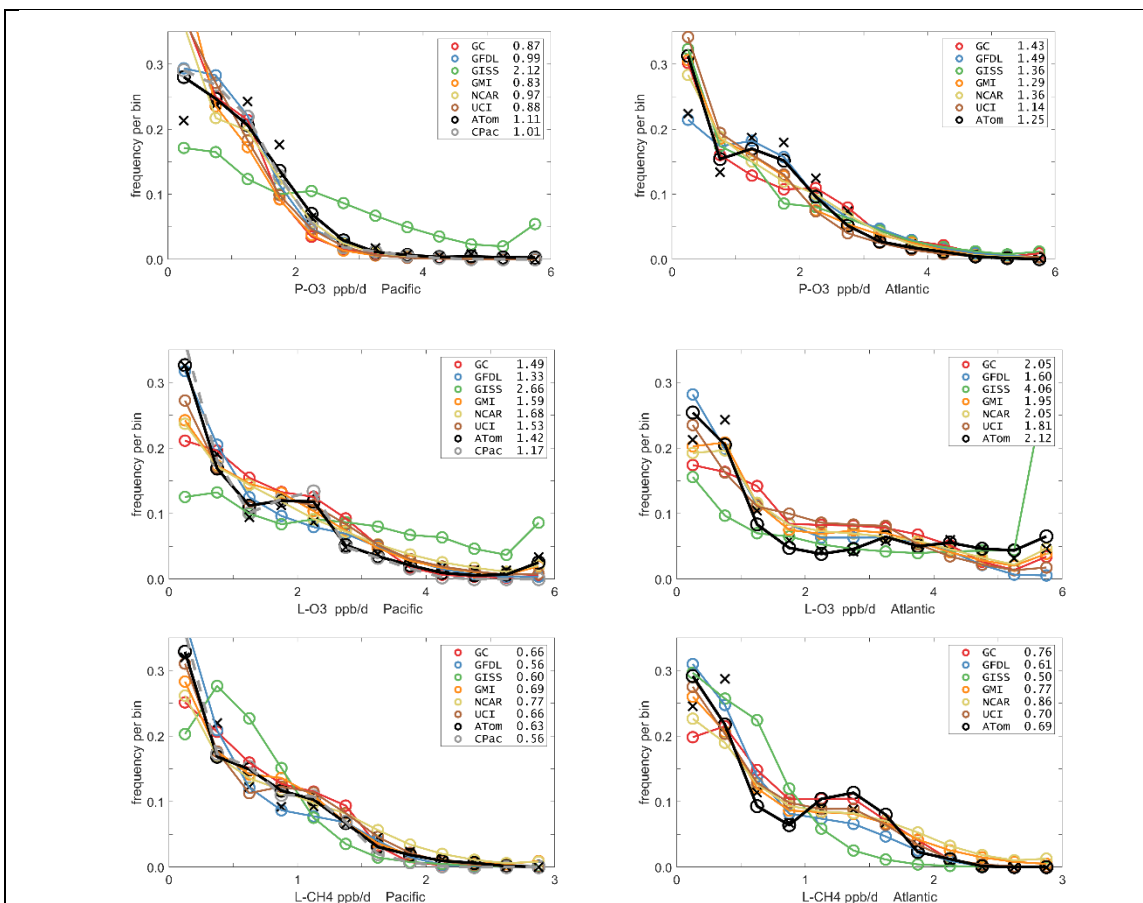
1006



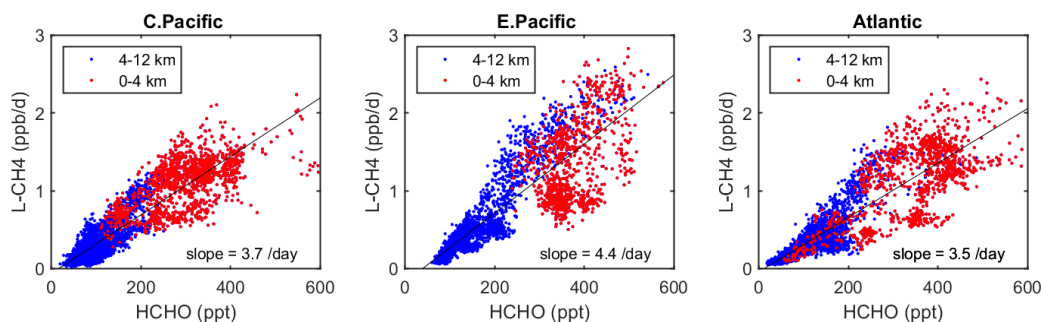
1014

1015 **Fig. 4** ~~Corr~~. Histograms of probability densities (PDs) of NO_x (0–12 km, row 1), NO_x (0–4 km,
1016 row 2), HOOH (0–12 km, row 3), and HCHO (0–12 km, row 4) for the three tropical regions
1017 (central Pacific, eastern Pacific, Atlantic). The ATom-1 data is plotted on top of the six global
1018 chemistry models' results for a day in mid-August and sampled as described in Fig. 3.

1019
1020



1021
 1022 **Fig. 5^{Corr.}** Probability densities (PD, frequency of occurrence) for the ATom-1 three
 1023 reactivities (rows: P-O3, L-O3, L-CH4 in ppb/day) and for the Pacific and Atlantic from 53° S to
 1024 60° N (columns left and right). Each air parcel is weighted as described in the text for equal
 1025 frequency in large latitude-pressure bins, and also by cosine(latitude). The ATom statistics are
 1026 from the UCIZ model, using MDS-2b and revised RDS* protocol (HNO₄ and PAN damping).
 1027 The Pacific results (solid black) also show the central Pacific alone (dashed gray). The six
 1028 models' values for a day in mid-August are averaged over longitude for the domains shown in
 1029 Fig. S1 in the Supplement, and then cosine(latitude) weighted. Mean values (ppb/day) are shown
 1030 in the legend. The PD derived from the ATom 10 s parcels binned into 1° latitude by 200 m
 1031 altitude (as shown for the tropics in Fig. 2) is typical of a high-resolution global model, and
 1032 denoted by black Xs.
 1033



1034
 1035
 1036
 1037
 1038
 1039
 1040

Fig. 6 ~~Corr.~~ Scatterplot of L-CH₄ (ppb/d) versus HCHO (ppt) for ATom 1 in the 3 tropical regions shown in Fig. 3. The air parcels are split into lower troposphere (0–4 km pressure altitude, red dots) where most of the reactivity lies and mid+upper troposphere (4–12 km, blue). A simple linear fit to all data is shown (thin black line) and the slope is given in units of 1/day.

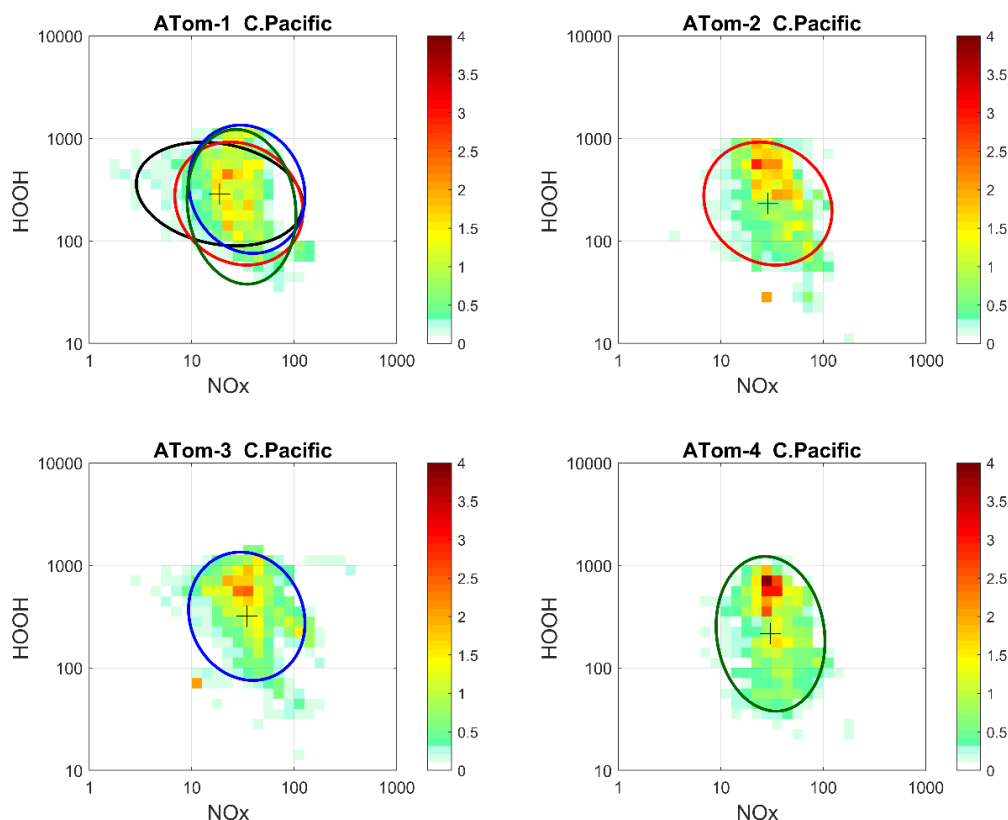


Fig. 7. 2D frequency of occurrence (PDs in log ppt mole fraction) of HOOH vs. NO_x for the tropical Central Pacific for all 4 ATom deployments. The cross marks the mean (in log space), and the ellipse is fitted to the rotated PD having the smallest semi-minor axis. The semi-minor and semi-major axes are 2 standard deviations of PD in that direction. The ellipses from ATom-2 (red), ATom-3 (blue), and ATom-4 (dark green) are also plotted in the ATom-1 quadrant.

1041

Used for	ID	Model name	Model type	Meteorology	Model Grid
clim	GFDL	GFDL-AM3	CCM	NCEP (nudged)	C180 x L48
clim, MDS-0	GISS	GISS-E2.1	CCM	Daily SSTs, nudged to MERRA	2° x 2.5° x 40L
clim, MDS-0/1	GMI	GMI-CTM	CTM	MERRA	1° x 1.25° x 72L
clim, MDS-0	GC	GEOS-Chem	CTM	MERRA-2	2° x 2.5° x 72L
clim, MDS-0	NCAR	CAM4-Chem	CCM	Nudged to MERRA	0.47° x 0.625° x 52L
clim, MDS-0 & 2b/1/2	UCI	UCI-CTM	CTM	ECMWF IFS Cy38r1	T159N80 x L60
MDS-0	F0AM	F0AM	box	MDS + scaled ATom Js	N/A

1042 The descriptions of models used in the paper. The first column denotes if the model's August
1043 climatology is used ('clim') and also the MDS versions used. F0AM used chemical mechanism
1044 MCMv331 plus J-HNO₄ plus O¹D)+CH₄. For the global models see P2017, P2017, and H2018.
1045

Table 2 Corr. Reactivity statistics for the three large domains (global, Pacific, Atlantic).										
Value	Region	Models using MDS-0								MDS-2b
		F0AM	GC	GISS	GMI	NCAR	UCI	U15	U97	UCIZ*
P-O3, mean, ppb/d	Global	2.12	2.12	2.57	2.08	2.22	2.38	2.37	2.37	1.23
	Pacific	1.96	2.00	1.99	e1.96	2.01	2.17	2.13	2.15	1.11
	Atlantic	1.96	2.12	3.49	2.20	2.44	2.48	2.48	2.49	1.25
L-O3, mean, ppb/d	Global	1.81	1.63	1.93	1.70	1.76	1.76	1.74	1.75	1.61
	Pacific	1.65	1.51	1.79	1.55	1.52	1.58	1.53	1.56	1.42
	Atlantic	2.15	2.02	2.37	2.17	2.47	2.28	2.28	2.30	2.12
L-CH4, mean, ppb/d	Global	0.81	0.76	0.43	0.75	0.73	0.79	0.78	0.78	0.61
	Pacific	0.85	0.82	0.40	0.80	0.79	0.82	0.80	0.81	0.63
	Atlantic	0.80	0.78	0.51	0.81	0.86	0.85	0.85	0.85	0.69
P-O3, %sum R in top 10%	Global	35%	32%	31%	32%	30%	34%	34%	34%	33%
	Pacific	34%	28%	28%	29%	29%	30%	30%	30%	27%
	Atlantic	24%	25%	24%	26%	24%	27%	27%	28%	27%
L-O3, %sum R in top 10%	Global	35%	35%	33%	35%	36%	36%	36%	36%	36%
	Pacific	33%	32%	29%	32%	31%	32%	32%	32%	32%
	Atlantic	28%	30%	29%	30%	34%	30%	30%	30%	29%
L-CH4, %sum R in top 10%	Global	33%	30%	27%	31%	31%	32%	32%	32%	30%
	Pacific	32%	28%	26%	29%	29%	29%	29%	29%	27%
	Atlantic	27%	25%	21%	26%	27%	27%	27%	27%	25%

1046

Global includes all ATom-1 parcels, Pacific considers all measurements over the Pacific Ocean from 53°S to 60°N, and Atlantic uses parcels from 53° S to 60° N over the Atlantic Ocean. All parcels are weighted inversely by the number of parcels in each 10° latitude by 100 hPa bin, and by cosine(latitude). Results from MDS-0 are shown because we have results from six models. Results from the updated MDS-2b are shown (UCIZ*) using the using the current UCI CTM model UCIZ and the RDS* protocol that preprocesses the MDS-2b initializations with a 24 h decay of HNO4 and PAN according to their local thermal decomposition frequencies, see text. See additional statistics in Table S8.

1047

Table 3. Cross-model RMS differences (RMSDs as % of mean) for the three reactivities.						
P-O3	F0AM	GC	GISS	GMI	NCAR	UCI
F0AM		48%	95%	45%	55%	42%
GC	48%		78%	26%	42%	32%
GISS	95%	78%		81%	72%	75%
GMI	45%	26%	81%		40%	35%
NCAR	55%	42%	72%	40%		42%
UCI	42%	32%	75%	35%	42%	(10%)
L-O3						
F0AM		40%	44%	43%	76%	38%
GC	40%		33%	25%	60%	24%
GISS	44%	33%		36%	66%	30%
GMI	43%	25%	36%		62%	28%
NCAR	76%	60%	66%	62%		60%
UCI	38%	24%	30%	28%	60%	(11%)
L-CH4						
F0AM		47%	136%	48%	82%	45%
GC	47%		111%	20%	60%	27%
GISS	136%	111%		114%	110%	121%
GMI	48%	20%	114%		57%	30%
NCAR	82%	60%	110%	57%		68%
UCI	45%	27%	121%	30%	68%	(14%)
<p>Matrices are symmetric. Calculated with the 31,376 MDS-0 unweighted ATom-1 parcels using the standard RDS protocol. F0AM lacks 5,510 of these parcels because there are no reported J-values. UCI shows RMSD between years 2016 (default) and 1997 as the value in parentheses on diagonal. The unweighted mean R from 3 core models (GC, GMI, UCI) are: P-O3 = 1.97, L-O3 = 1.50, L-CH4 = 0.66, all ppb/d. The three core-model RMSDs with respect to one another are less than 36% and boldened.</p>						

1048

1049

Table 4 Corr. ATom data files used here		
Primary Aircraft Data	Formatting and content	Comments
(a) Mor.all.at1234.2020-05-27.tbl (b) Mor.WAS.all.at1234.2020-05-27.tbl (c) Mor.TOGA.all.at1234.2020-05-27.tbl All from Wofsy et al., 2018.	(a) 149133 records x 675 csv columns, 10 s merges of flight data plus chemistry & environmental measurements (b) 6991 records x 729 csv columns, 30-120 s intervals to fill flasks (c) 12168 records x 727 csv columns, 35 s intervals of instrument	Core source of ATom measurements. irregular and difficult formatting; extremely long ascii records; large negative integers or 'NA' for some non-data.
Modeling Data Stream (MDS-2b)		
(a) MDS_DC8_20160729_R3.ict (b) MDS_DC8_20170126_R4.ict (c) MDS_DC8_20170928_R4.ict (d) MDS_DC8_20180424_R4.ict (e) ATom_MDS.nc Derived here. Corrigenda (af) ATom_MDS2b.nc Note: The .ict files are not corrected	(a) netcdf file containing regularly spaced 10 s observations for ATom-1 (-32383 records), x 87 csv columns, 10 s intervals of chemical & other data, plus flags to indicate gap-filling (b) ATom-2 (-33424 records), x 87 csv columns (c) ATom-3 (-40176 records), x 87 csv columns (d) ATom-4 (-40511 records), 146,494 in total; includes physical flight data (11), chemical data (39), miscellaneous data including corrected HNO4 and PAN (6), flag data (50), x 87 csv columns (e) ATom MDS-2 & MDS-2b in netcdf	Regular formatting; all data gap filled <u>with flags to identify the method and extent of filling</u> ; NaN's only for flight 46; for use in modeling of the chemistry and related statistics from the ATom 10 s data.
Reactivity Data Stream (RDS*-2b)		
(a) RDS_DC8_20160729_R1.ict (b) RDS_DC8_20170126_R1.ict (c) RDS_DC8_20170928_R1.ict (d) RDS_DC8_20180424_R1.ict (e) ATom_RDS.nc Derived here. Corrigenda (f) ATom_RDS2b.nc Note: The .ict files are not corrected	(a) netcdf file containing regularly spaced reactivities for 10 s parcels from ATom-1234 (146,494 in total); includes latitude, longitude and pressure of model grid cell used in the calculation; includes P-O3, L-O3, L-CH4, L-CO, J-O1D, plus dO3/dt = net O3 change over 24 h. Reactivities are given for 5 days separated by 5 days in the middle of each deployment, plus the 5-day mean. (a) ATom-1: 32383 records x 16 csv columns, 10 s intervals of flight data, modeled reactivities & J-values plus 5-d std dev (b) ATom-2: 33424 records x 16 csv columns (c) ATom-3: 40176 records x 16 csv columns (d) ATom-4: 40511 records x 16 csv columns (e) ATom RDS: all UCI-CTM data in netcdf	Results from newest results from UCI-CTM only; using RDS* protocol and MDS-2; NaN's only for flight 46; for use analyzing the reactivities from the ATom 10 s data. Corrigenda: New-UCI CTM version (UCIZ) corrects mistakes in the reaction rates; it is run with RDS* protocol (<u>PAN and HNO4 decay</u>) and using MDS-2b. <u>NaN's only for flight 46.</u>